NASA Contractor Report 189672

Control-Structure Interaction/Mirror Motion Compensation

Mark McLaren, Peter Chu, and Xen Price

Space Systems/Loral
Palo Alto, California

Contract NAS1-19242
September 1992

National Aeronautics and Space Administration

Langley Research Center
Hampton, Virginia 23665-5225

MSOSS Task 1

CONTROL-STRUCTURE INTERACTION/ MIRROR MOTION COMPENSATION

Final Report

Mark McLaren
Peter Chu
Xen Price

Objective

Space Systems/LORAL (formerly Ford Aerospace, Space Systems Division) has implemented a rigid-body Mirror Motion Compensation (MMC) scheme for the GOES-I/M spacecraft currently being built for NASA and NOAA. This has resulted in a factor of 15 reduction in pointing error due to rigid-body spacecraft motion induced by the periodic black-body calibration maneuvers required for the instruments.

GOES MMC considers the spacecraft and the payload mirrors as rigid bodies. The structural flexibility effects are small and are included in the total pointing budget as a separate item.

For other large multi-payload platforms, the structural flexibility effects can be more important in sensor pointing jitter as the result of payload motion. The objective of the current task is to extend the GOES MMC concept to also compensate for the structural flexibility effects and demonstrate the technique on such spacecraft.

Objective

- Extend rigid-body Mirror Motion Compensation (MMC) to include structural flexibility effects.

- Study MMC performance in platforms where payload pointing jitter due to structural flexibility is significant.

MMC Concept

- Spacecraft disturbances cause payload pointing errors.
- Pointing error from deterministic disturbances can be calculated.
- Calculated pointing error is fed to payload LOS controller and compensated.
- GOES-I/M corrects rigid-body pointing errors only.
- GOES-I/M pointing errors from mirror motion/structural flexibility interactions are small.

MMC Concept

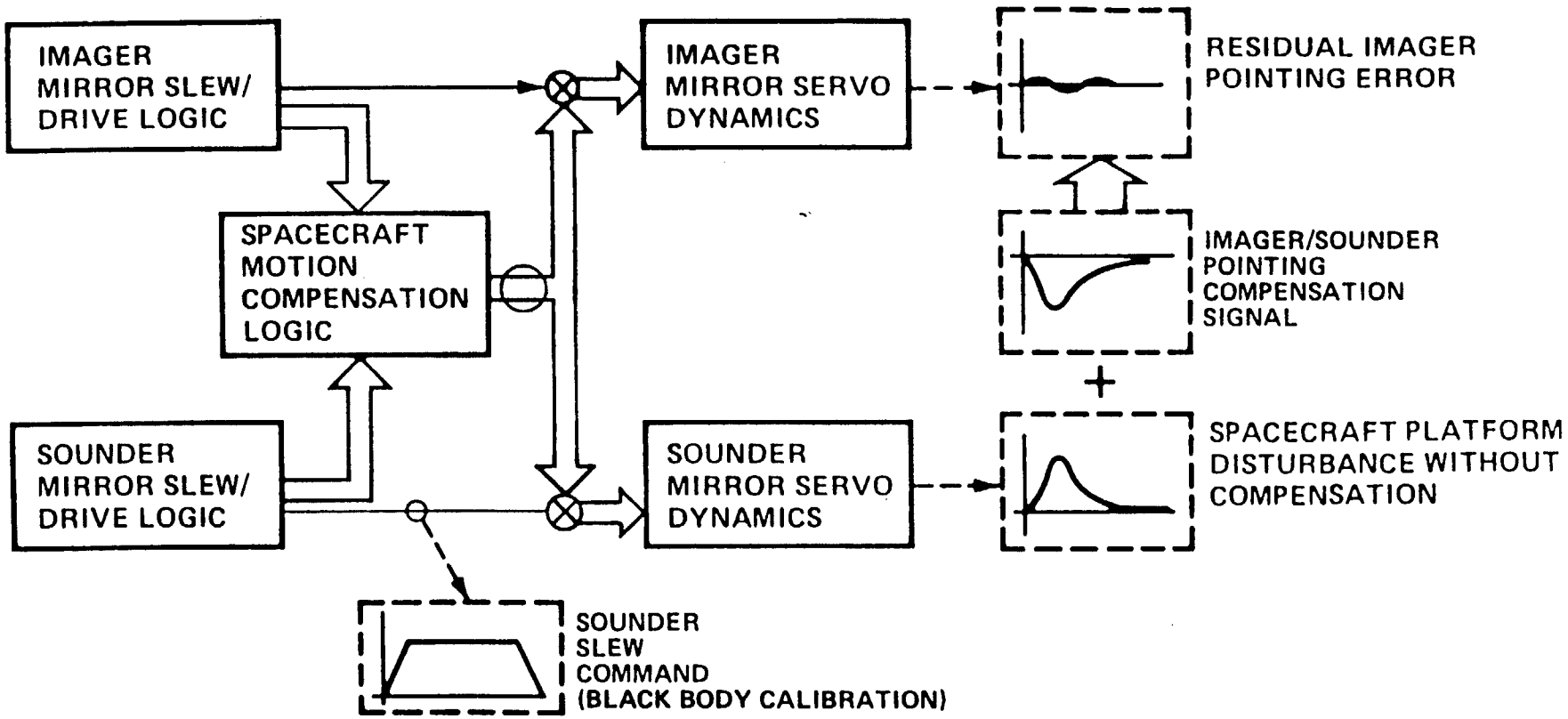
IMAGER MIRROR SLEW/ DRIVE LOGIC
IMAGER MIRROR SERVO DYNAMICS
RESIDUAL IMAGER POINTING ERROR
SPACECRAFT MOTION COMPENSATION LOGIC
IMAGER/SOUNDER POINTING COMPENSATION SIGNAL
+
SOUNDER MIRROR SLEW/ DRIVE LOGIC
SOUNDER MIRROR SERVO DYNAMICS
SPACECRAFT PLATFORM DISTURBANCE WITHOUT COMPENSATION
SOUNDER SLEW COMMAND (BLACK BODY CALIBRATION)

Project Scope

- Design a low-order rigid-body MMC controller and extend the MMC technique to compensate for one, two, and three structural modes with a single disturbance scenario
  - Assess residual pointing error as a function of rigid-body and flexible mode parameter variations.
  - Apply different disturbance scenarios and reassess.
- As a baseline for comparison, design a rigid-body MMC controller for the UARS spacecraft.
- Extend the UARS rigid-body MMC controller to incorporate flexible-body effects using concepts developed with the low-order model.
- Consider the impact of upgrading the remote sensors with larger scanning mirrors (therefore larger disturbances), and evaluate how the larger disturbances might translate into MMC errors.
- Investigate the benefit of incorporating sensor measurements and feedback into the MMC scheme to improve robustness and reduce the dependency on the CSI analytical model fidelity.
- Summarize results and make recommendations regarding the application of MMC techniques to
  - future upgraded GOES-Next class spacecraft
  - UARS/EOS class spacecraft
  - evolutionary Space Station Freedom class of spacecraft
- Identify areas where CSI technology application would be most beneficial and propose areas for future CSI benefits tasks.

Project Scope

- Extend MMC to flex effects on low-order model.
- Design flexible mode MMC for UARS class spacecraft.
- Assess sensitivity of modeling error.
- Evaluate impact of larger scanning mirrors.
- Incorporate sensor feedback to reduce sensitivity.
- Make recommendations on use of MMC to future GOES, UARS/EOS, and Space Station classes of platform.

Approach

The GE torque disturbance simulations were reproduced to verify the NASTRAN model and simulation setup. From these simulations, the combination that produced the largest pointing error was selected for further analysis. In this case, this occurred at the WINDII (Wind Imaging Interferometer) LOS due to the MLS (Microwave Limb Sounder) scan 3 profile cycles.

A rigid-body MMC (MMC using only rigid-body mode compensation) was performed on the UARS spacecraft to provide a response baseline, to which was compared the response after MMC incorporating flexible-modes in addition to rigid-body modes.

The performance of the MMC incorporating flexible-body modes is degraded by various modelling uncertainties. A sensitivity analysis was conducted to evaluate the specific effect to variations in the various flexible-mode parameters used in the MMC.

Approach

- Establish UARS uncompensated pointing error as baseline
- Choose worst case disturbance / pointing requirement pair
- Develop rigid-body MMC on UARS
- Develop flexible-body MMC on UARS
- Take variations of parameters in MMC
  - modal frequency
  - modal magnitude
  - modal damping
  - time delay

  and assess effects on residual error
- Determine limitations on MMC performance

Approach (cont.)

As the size of the slewing payload increases, the resulting disturbances also increase. The functional relationship between the payload size and the disturbance effects is developed, and an example case for UARS with a larger payload is presented.

The current UARS rigid-body controller is implemented. Since the rigid-body controller has a very low bandwidth, it will affect only the long-term rigid-body response, but should not affect the flexible mode response.

The performance of the system with feedback of sensor (gyro) measurements is compared to that of the feedforward scheme (MMC) alone. This comparison includes common feedback error sources such as time delay and sensor noise.

If sensor measurents are available, is MMC required? The answer to this question depends on certain conditions regarding sensor performance and availability. Several circumstances when it is appropriate to consider feedback and MMC working together to acheive the pointing and jitter requirements are outlined.

Approach (cont.)

- Increase disturbing payload dimensions and determine effect on disturbance response
- Consider rigid-body controller effect on flexible response
- Consider performance of sensor feedback c.f. MMC
- Consider sensor measurements and MMC synergism

UARS Spacecraft

This slide shows a schematic of the UARS spacecraft. The WINDII (Wind Imaging Interferometer) and MLS (Microwave Limb Sounder) instruments, among others, are labeled.

Traditionally the MMC is applied to the instrument LOS controller to remove the disturbance input. However, note that the WINDII instrument does not have any mechanical LOS control, so the MMC would have to be applied electronically or in post-processing.

UARS Spacecraft

ASTRO SPACE DIVISION

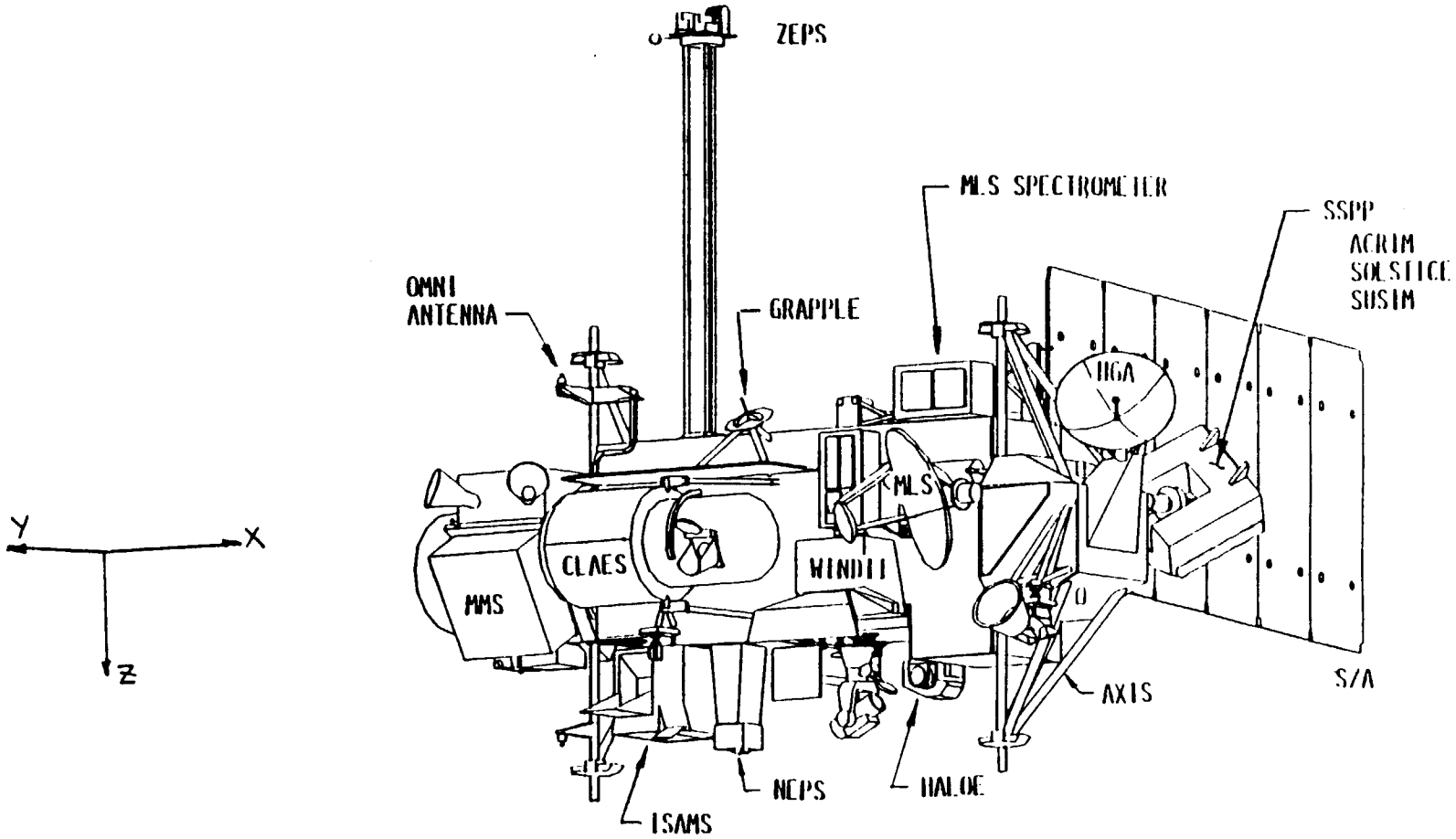

(1) The NASTRAN analysis builds up the mass and stiffness matrices from finite elements, and evaluates the modal frequencies and mode shapes of the model. Damping is omitted in these evaluations at this stage of modelling to enable full modal decoupling. This can only be achieved with real modes if in addition there is little or no bias momentum.

(2) The modal coordinate form of the equations are fully decoupled. Inherent to this description is the assumption that the response can be broken into independent temporal and spatial parts.

(3) The physical output coordinates are the rotations of the nodes represented in the finite element model. They are found as the sum of the individual modes whose magnitudes are determined by modal shape.

(4) The response of the system to the input **Q** can be determined as the sum of the responses of the individual modes to the same input, i.e. by superposition. This is the pole-residue formulation, and is the basis for all simulations performed in this work.

Note that all these equations are essentially transformed varieties of the same equation. Modal damping is added at the level of equation (4).

Simulation Methodology

(1) NASTRAN Analysis:

$$M\ddot{\mathbf{y}}(t)+K\mathbf{y}(t)=\mathbf{Q}(t)$$

(2) Modal coordinate form:

$$\ddot{\eta}(t)+\left[\omega^2\right]\eta(t)=P^T\mathbf{Q}(t)$$

(3) Physical output coordinates:

$$\mathbf{y}(t)=P\eta(t)=\sum_{j=1}^{m}\mathbf{p}_j\eta_j(t)$$

(4) Frequency domain response:
(pole-residue formulation)

$$\mathbf{y}(s)=\sum_{j=1}^{m}\left[\frac{\mathbf{p}_j}{s^2+2\zeta_j\omega_j s+\omega_j^2}\right]P^T\mathbf{Q}(s)$$

MLS Scan 3 Disturbance Profile

- The MLS 3 scan pulse cycle consists of 27 forward torque pulse pairs followed by 2 return torque pulse pairs, about the spacecraft X-axis, all separated by 2.048 sec. Each torque pulse pair is equivalent to one position step ("step and dwell" instrument motion). Total MLS instrument one-way travel is about 1.32 degrees.

- For a forward torque pulse pair,

  - second pulse begins Tf=0.062 sec after beginning of first pulse
  - total duration is 0.078 sec
  - pulse widths 2T and T sec (T=0.016 sec)
  - pulse magnitudes A and -2A (A=31.92 lb-in)

- For a return torque pulse pair,

  - second pulse begins Tr=0.737 sec after beginning of first pulse
  - total duration is 0.753 sec
  - pulse widths 2T and T sec (T=0.016 sec)
  - pulse magnitudes -A and 2A (A=31.92 lb-in)

- Each pulse cycle lasts approximately 58 seconds and the cycle is repeated approximately every 67.6 seconds. Each of the two pulse pairs produce a net torque of zero, so that the rigid-body response is constant between the individual pulse pairs of the sequence. This is a "step and dwell" scan profile rather than a continuous slew profile.

MLS Scan 3 Disturbance Profile

One MLS scan 3 cycle consists of 27 forward pulses and 2 return pulses.

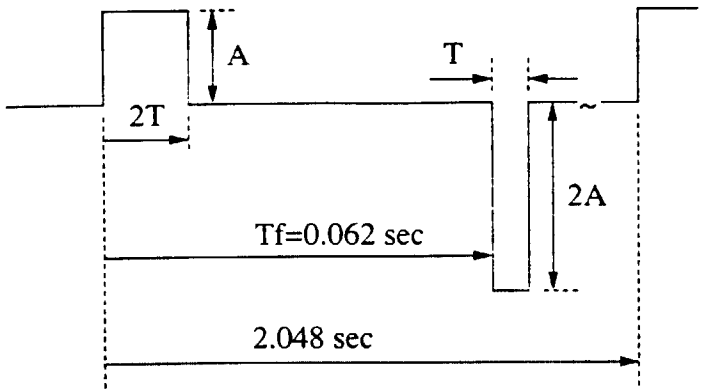

Forward pulse

Tf=0.062 sec
T=0.016sec
A=31.92 lb-in

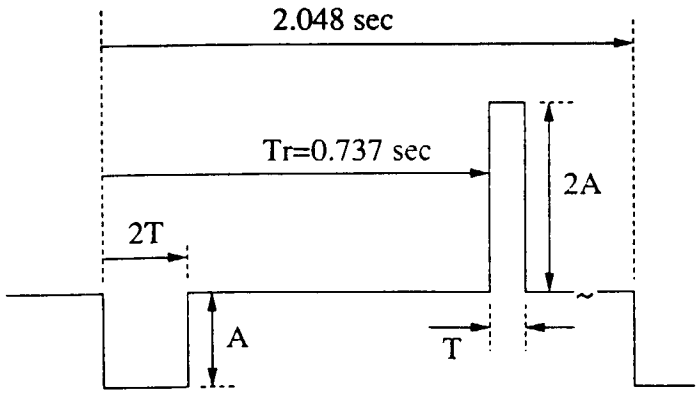

Return pulse

Tr=0.737 sec
T=0.016 sec
A=31.92 lb-in

The input function is a series of forward torque pulse pairs followed by a series of return torque pulse pairs. For the MLS scan 3 profile, the input DOF (point of disturbance) is the X-axis rotation of grid location 40513 (DOF 96 in the mode shapes). The MLS scan profile is repeated at regular intervals, so that repeated scans will be simulated to illustrate the effect of initial conditions on the pulse cycles.

The response equations are a sum over all modes of the individual modal responses to the series of forward and return pulses, scaled by the input and output modal amplitudes. The WINDII output DOF's are the X-axis rotations of grid locations 110001, 110005, 110007, and 110042 (DOF's 79, 82, 85, and 88 in the mode shapes). The overall WINDII response at any time is taken as the maximum response at any of these DOF's at that time. In fact, the output at DOF 88 has the maximum output in almost every case.

The simulations determine the response for each mode to one forward torque pulse pair and one return torque pulse pair. The response of each mode to the full sequence of torque pulses is determined by time shifting the associated single pulse response and superposition.

Response to MLS Scan 3 Disturbance

- Input function

$$P^T \mathbf{Q}(t) = \left(P^T\right)_i q(t)$$

$$q(t) = \sum_{k=1}^{n_f} q_f(t - t_k) + \sum_{k=n_f+1}^{n_f+n_r} q_r(t - t_k)$$

- Response equations

$$\mathbf{y}(t) = \sum_{j=1}^{m} p_{ij} \mathbf{p}_j \left[\sum_{k=1}^{n_f} x_{j_f}(t - t_k) + \sum_{k=n_f+1}^{n_f+n_r} x_{j_r}(t - t_k) \right]$$

Rigid-Body Response

This slide shows the rigid-body response only at WINDII to 2 MLS scan 3 torque pulse cycles. Note the "step and dwell" nature of the response following the similar nature of the disturbance input.

Each torque pulse pair is a step in the WINDII response (pointing error). Each forward torque pulse pair causes a WINDII error step of approximately +0.07 arcsec. Each return torque pulse pair causes a WINDII error step of approximately -0.96 arcsec. The large return pulse steps are due to the longer torque pulse pair separation time in the return pulse that allows a longer coasting phase of the MLS motion.

Rigid-Body Response

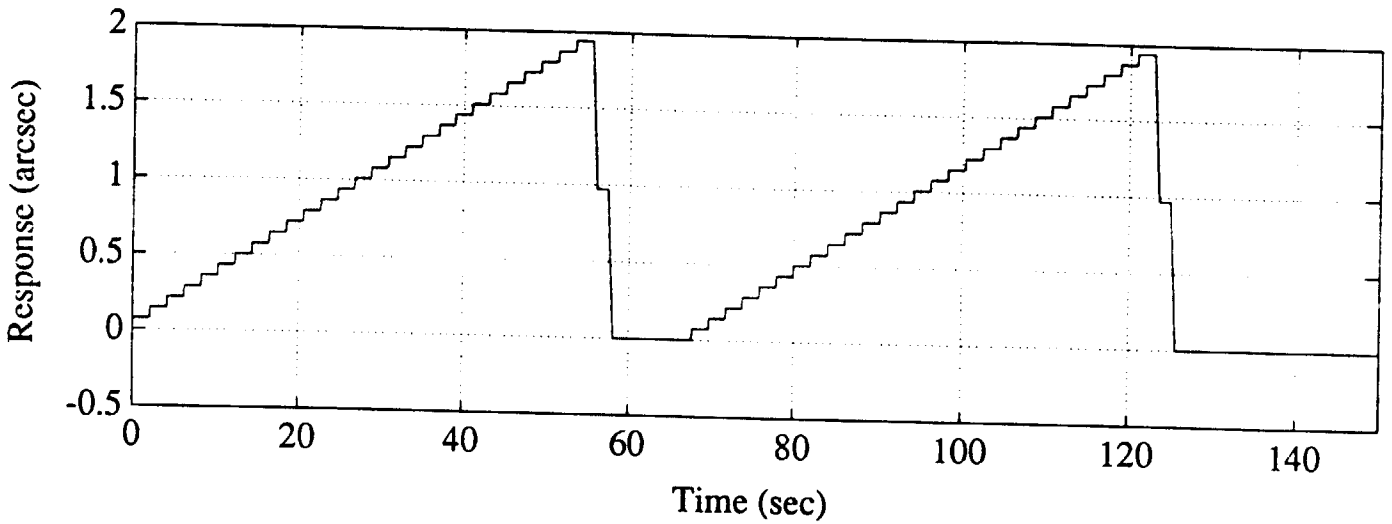

Rigid-Body Response Equations

The rigid-body response to one (forward or return) torque pulse pair can be determined analytically in four parts: during and after the two pulses of the forward or return pulse pair. This partitioning is required since the individual pulse widths (T and 2T) are not small with respect to the pulse separations Tf and Tr (i.e. we cannot approximate the pulses as impulses).

The final constant value of the rigid-body response is determined by the length of the first pulse and the time span between the pulses. This is the period of constant angular velocity for the spacecraft caused by the first torque pulse.

The equations shown are valid for either a forward or return pulse pair, where Ts is replaced by the appropriate Tf or Tr. In these equations, any spacecraft control is ignored, since it is assumed that the stop/dwell time is much shorter than the control system time constant.

Rigid-Body Response Equations

Response to one forward or return pulse pair

$$x_j(t) = \begin{cases} \frac{1}{2} A t^2 & \forall t \varepsilon [0, 2T) \\ 2AT(t-T) & \forall t \varepsilon [2T, T_s) \\ 2AT(t-T) - A(t-T)^2 & \forall t \varepsilon [T_s, T_s + T) \\ AT(2T_s - T) & \forall t \geq T_s + T \end{cases}$$

Baseline Pointing Error

This plot shows the baseline pointing error (X-axis response at WINDII to two MLS scan 3 pulse cycles). The baseline error is the response before MMC compensation, and is the sum of the rigid-body and flexible-mode responses.

The maximum error at WINDII due to the repeated 1.32 degree MLS slews is approximately 2.7 arcsec. The total error at WINDII due to the MLS scan 3 motion is reduced by a factor of approximately 2 by the removal of the rigid-body response (from 2.7 arcsec to 1.2 arcsec).

The actual baseline pointing error was established using a simulation of many repeated MLS scan cycles, although the chart here only shows a sequence of 2 for clarity.

Baseline Pointing Error

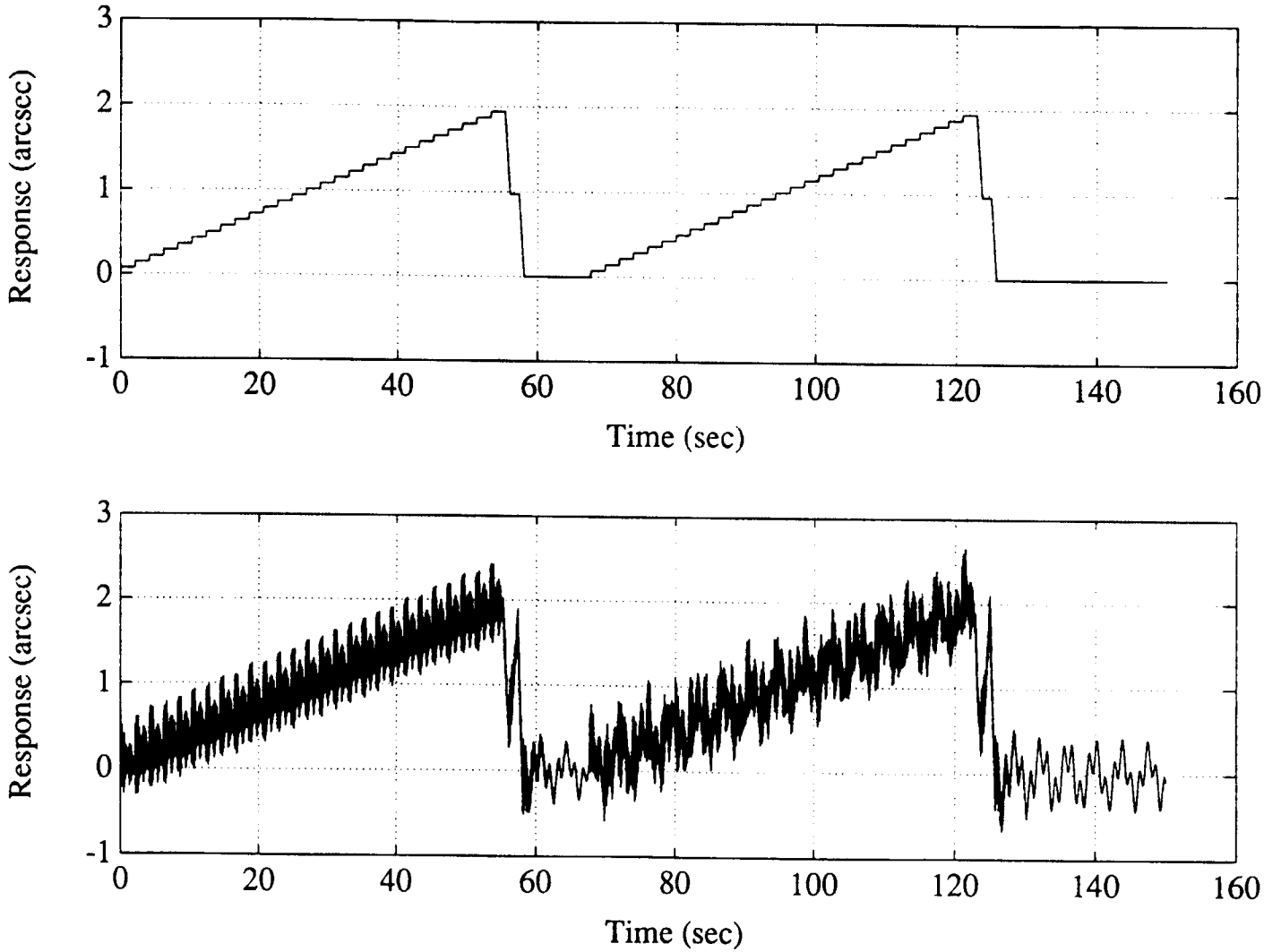

Shown is a block diagram of the MMC for UARS.

The commanded torque is applied to the MLS instrument and provides the disturbance torque on the S/C main body that is seen at WINDII as a pointing error. The commanded torque is intercepted and also sent to the MMC system. This system includes models of the system dynamics and actuator/sensor dynamics, and calculates the expected WINDII disturbance due to the commanded MLS torques. This expected WINDII disturbance is transformed into the appropriate WINDII actuator commands to nullify the expected error.

In the current work, we assume perfect MLS and WINDII actuators, although models of these devices could be easily included if information on them was available.

MMC for UARS

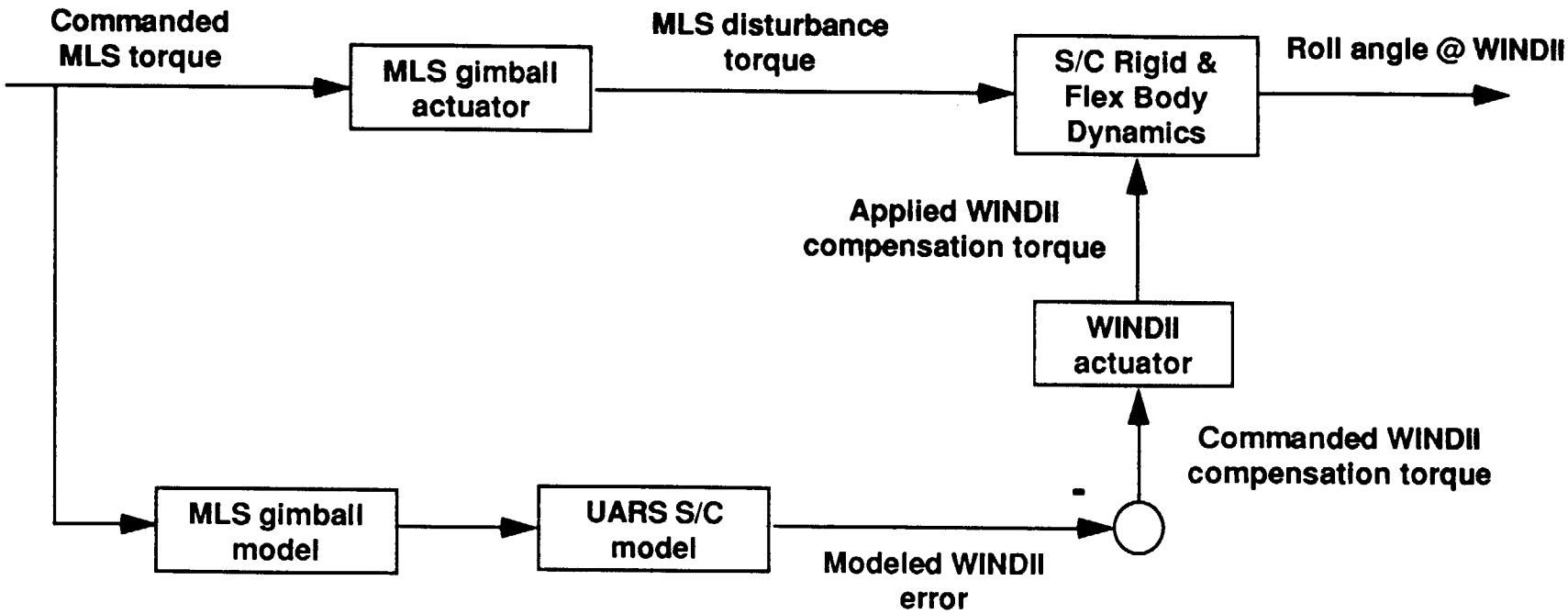
Commanded
MLS torque
MLS gimball
actuator
MLS disturbance
torque
S/C Rigid &
Flex Body
Dynamics
Roll angle @ WINDII
Applied WINDII
compensation torque
WINDII
actuator
Commanded WINDII
compensation torque
-
MLS gimball
model
UARS S/C
model
Modeled WINDII
error

Pointing Error After Rigid-Body MMC

This plot shows the residual pointing error at WINDII after the rigid-body MMC has been applied assuming perfect model knowledge and compensation actuation. The remaining response is therefore due entirely to the flexible-body response induced at WINDII by the MLS scan 3 cycles. The effect from each of the 27 forward pulses and 2 return pulses in each pulse sequence can be clearly seen, especially during the first scan cycle.

Note that the second scan sequence shows more response than the first. This is due to the flexible-mode motion remaining from the return pulse excitation when the second MLS pulse cycle begins. The effect of initial conditions can be seen to increase the peak of the flexible-mode response by approximately 25% over that when the initial conditions are zero. The effect of initial conditions on the response normally reaches near steady-state after 2-3 pulse sequences.

Pointing Error After Rigid-Body MMC

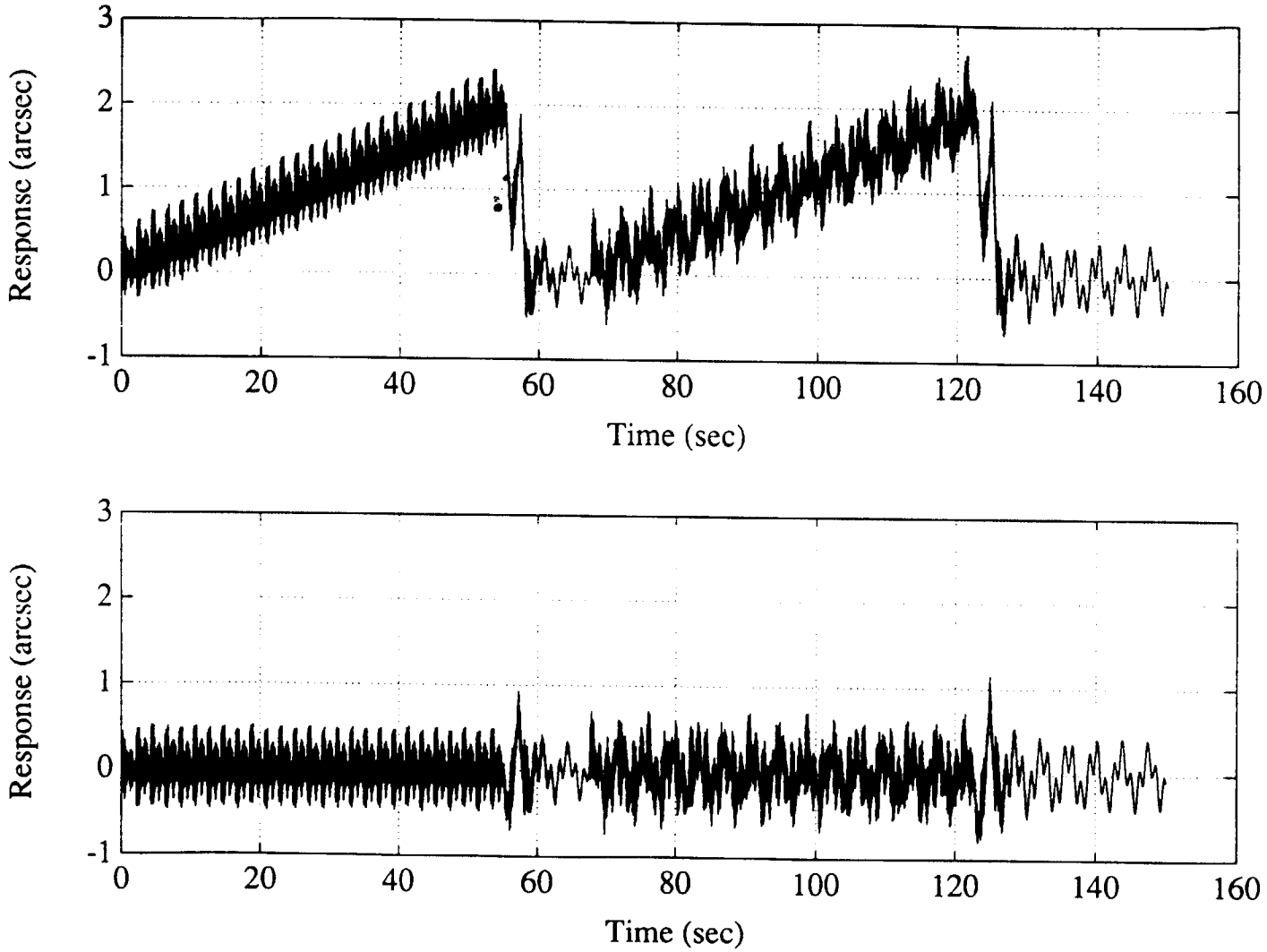

Which Flexible Modes to Compensate?

The flexible-body MMC approach is to remove the flexible-body response in the same manner as the rigid-body response was removed - by feedforward MMC. The question to be answered is:

"How many and which modes should be included in the MMC implementation?"

Only those modes that significantly contribute to the pointing error need be considered as candidates for compensation.

We must consider the specific modal response at a particular location due to a particular disturbance input. The modal response to a general pulse pair was given previously. This enables us to generate a modal ranking based on the specific MLS scan 3 timing parameters and WINDII response nodes.

The equation shown here is the frequency domain response equations for mode **j** to a sequence of **nf** forward pulses and **nr** return pulses separated by **T1** seconds, with the sequence repeated every **T2** seconds a total of **ns** times. The forward and return pulse parameters T,Tf, and Tr are as defined earlier.

Which Flexible Modes to Compensate?

- Only need compensation for most dominant modes
- "Dominance" based on usual kind of modal importance criteria but tailored to frequency content of disturbance profile.
- Frequency response to repeated MLS scan 3 cylces is:

$$\mathbf{y}_j(s) = \frac{Ap_{ij}\mathbf{p}_j}{s\left(s^2+2\zeta_j\omega_j s+\omega_j^2\right)}\sum_{\ell=0}^{n_s-1} e^{-s\ell T_2}\left\{\left[1-e^{-2sT}-2e^{-sT_f}+2e^{-s(T_f+T)}\right]\sum_{k=0}^{n_f-1} e^{-skT_1}+\right.$$

$$\left.-\left[1-e^{-2sT}-2e^{-sT_r}+2e^{-s(T_r+T)}\right]\sum_{k=n_f}^{n_f+n_r-1} e^{-skT_1}\right\}$$

Modal Residue Scaling

This plot shows the modal residue scaling. Each point represents for one mode the product of the mode shape elements corresponding to the input and output DOF's. For each of the 268 non-zero modal frequencies in the UARS model, the value plotted is the maximum value of this modal residue for the X-axis input DOF 96 and X-axis output DOF's 79, 82, 85, 88. In general, output DOF 88 exhibits the maximum response over all the WINDII response DOF's.

This is usually the measure by which modal importance is judged. However, for MMC it does not use all the available information since the mirror motion profile is very specific and its frequency content may particularly excite some flex modes and make them much more important.

Modal Residue Scaling

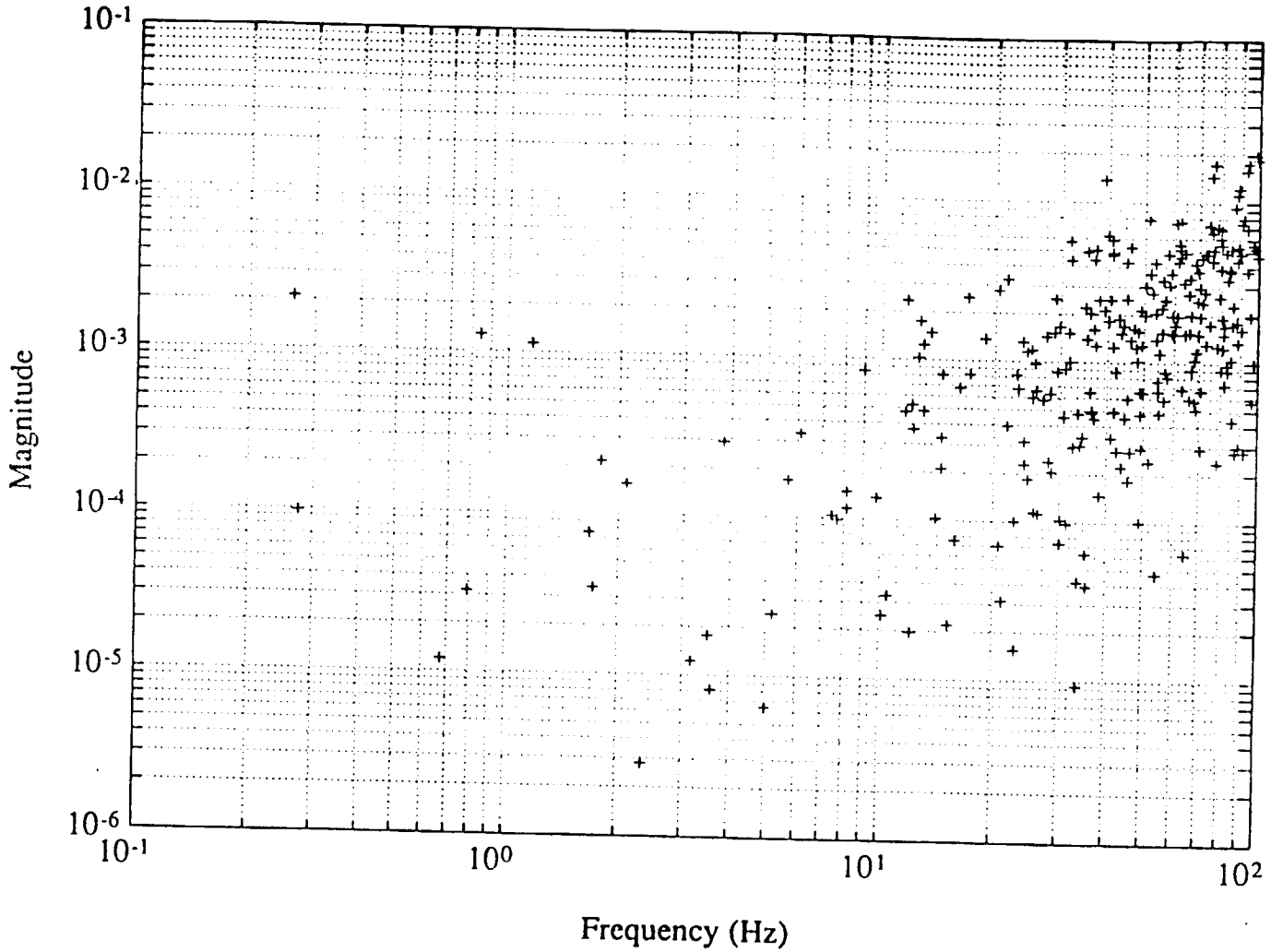

Modal Frequency Weighting

This plot shows the frequency dependent weighting of the modal response equations shown on the previous slide. This plot is for a sequence of 256 MLS scan 3 pulse cycles. This is enough pulse sequences so that the frequency weighting has approximately reached a steady-state condition.

Modal Frequency Weighting

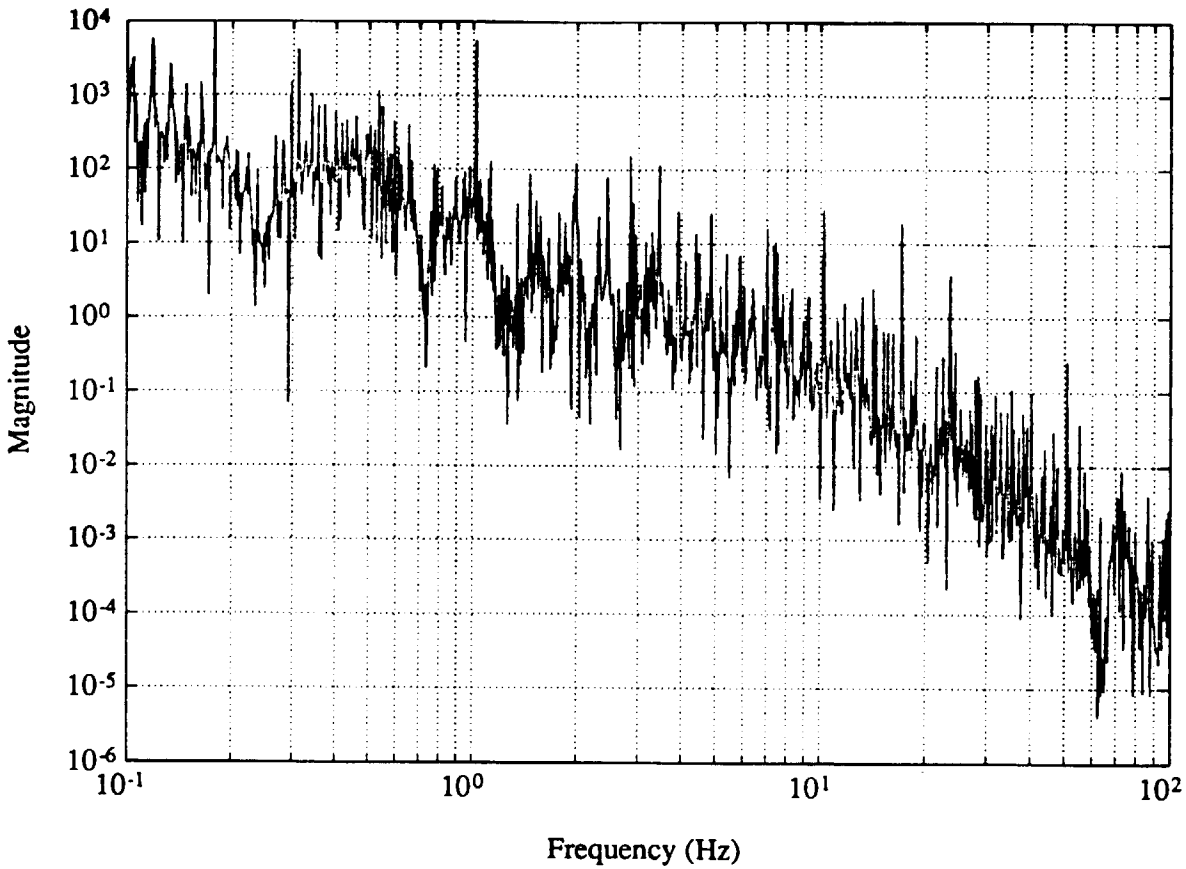

Modal Importance at WINDII to Repeated MLS Scan 3 Cycles

This plot shows the combined effect of the modal residue scaling and the modal frequency weighting. Those modes with the largest magnitudes are the most important modes with respect to the specific input and outputs under consideration. This plot indicates that there are relatively few modes that individually contribute in a significant way to the pointing error, although the cumulative sum of many apparently insignificant modes may be significant.

It is important to note that this ranking is specific for the input/output combination of MLS scan 3 cycles and WINDII pointing error. It is also important to note that the plot is on a log-log scale. If it were plotted on a linear scale, the dominant modes would seem much more dominant.

Modal Importance

- at WINDII to repeated MLS scan 3 cycles.

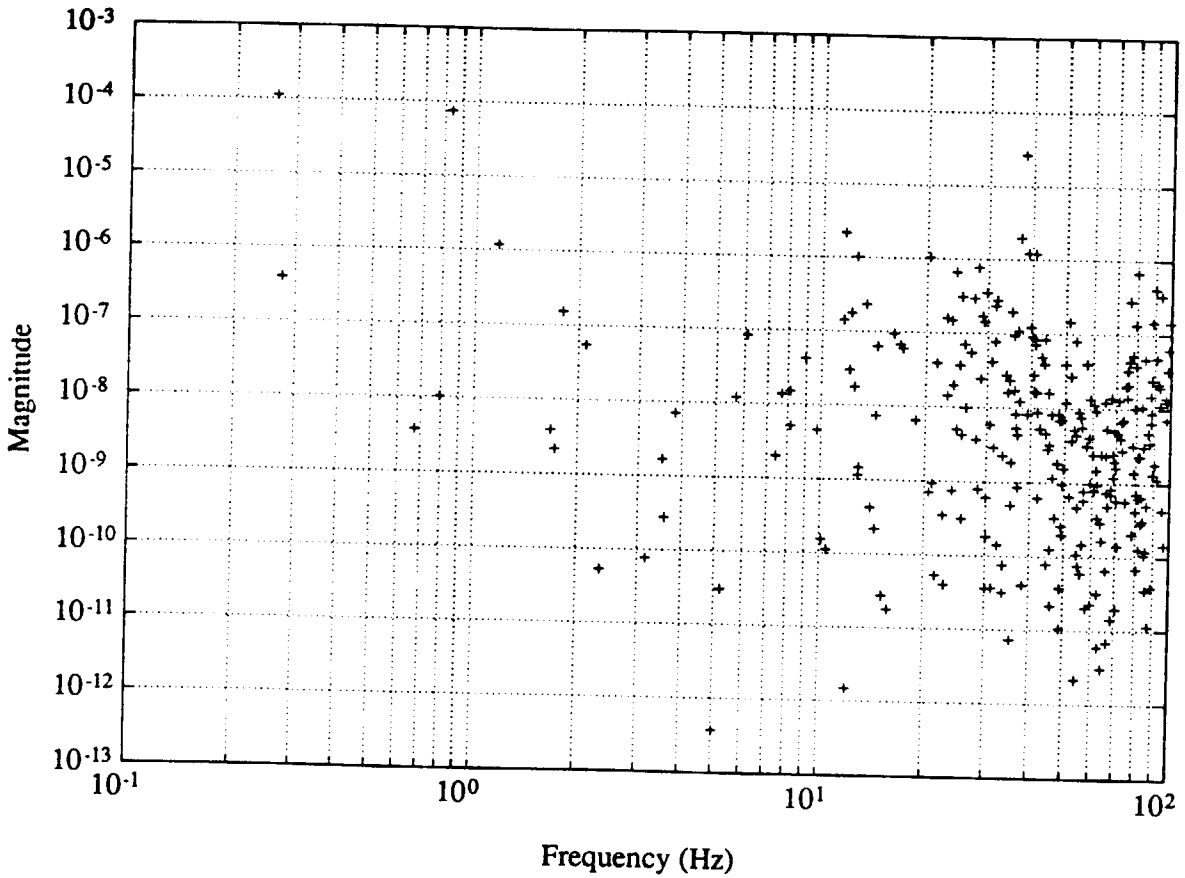

Modal Ranking for MMC

This table shows the 10 most important modes in the WINDII response to 256 repeated MLS scan 3 pulse cylces, as predicted by the previous analysis. Modes 7 and 11 are the most important low frequency modes, and are included in the MMC.

The mode at 38 Hz takes 3rd place in importance. It is clear that the mode should not be compensated, because we have no confidence in the NASTRAN model to correctly predict that there is indeed anything in that region worth considering. Also, its frequency is simply too high to be handled by a spacecraft control system.

The modal ranking measure indicated is the magnitude of the individual modal responses normalized to the most important mode - mode 7.

Modal Ranking for MMC

Modal Ranking	Mode #	Frequency (Hz)	Normalized modal importance
1	7	0.263	1.0000
2	11	0.8429	0.6691
3	113	38.026	0.2379
4	35	11.655	0.0191
5	111	37.122	0.0173
6	115	39.074	0.0110
7	120	40.955	0.0106
8	12	1.1658	0.0105
9	54	20.39	0.0094
10	40	12.607	0.0092

Flexible-mode MMC cutoff

Flexible Mode MMC

Only the effects of flexible modes 7 and 11 (at 0.263 Hz and 0.843 Hz respectively) were compensated based on the modal dominance analysis just given.

This sequence of plots shows the cummulative effect on the residual error of rigid-body MMC flexible mode 7 and 11 MMC, with perfect model knowledge and compensation actuation assumed. The first plot is the baseline error, the second plot is after the rigid-body MMC, and the last plot is after the addition of the two-mode flexible mode MMC. The pointing error has been reduced by a factor of 2.5 over the error remaining after the rigid-body response alone was removed (from 2.7 arcsec nominal, to 1.2 arcsec after rigid-body, to 0.5 arcsec after 2 mode MMC). This is achieved with only 2 flexible modes added to the MMC. Note that the unsymmetric nature of the bottom plot is an artifact of the plotting - there are physical limitations to how many points per plot the printer can accept, and some of the peaks were not included for this plot. However, a closer examination of the plot (with a larger x-axis scale for example) shows that the response with 2 mode MMC is approximately symmetric about the response = 0 axis.

Adding mode 113 MMC (assuming this is advisable) confirms the modal dominance analysis and shows that this mode individually does not contribute very significantly to the overall residual pointing error due to these disturbances. However, even if the potential effect of mode 113 was more significant, it seems impractical to attempt compensation of such a high frequency mode because of the extreme uncertainty in the NASTRAN analysis. Typically, NASTRAN results for any but a few lowest frequency modes are highly suspect.

Of course, including all modes in the MMC should (and does) result in zero pointing error (since we are assuming no actuation dynamics and perfect modelling).

Flexible-Mode MMC

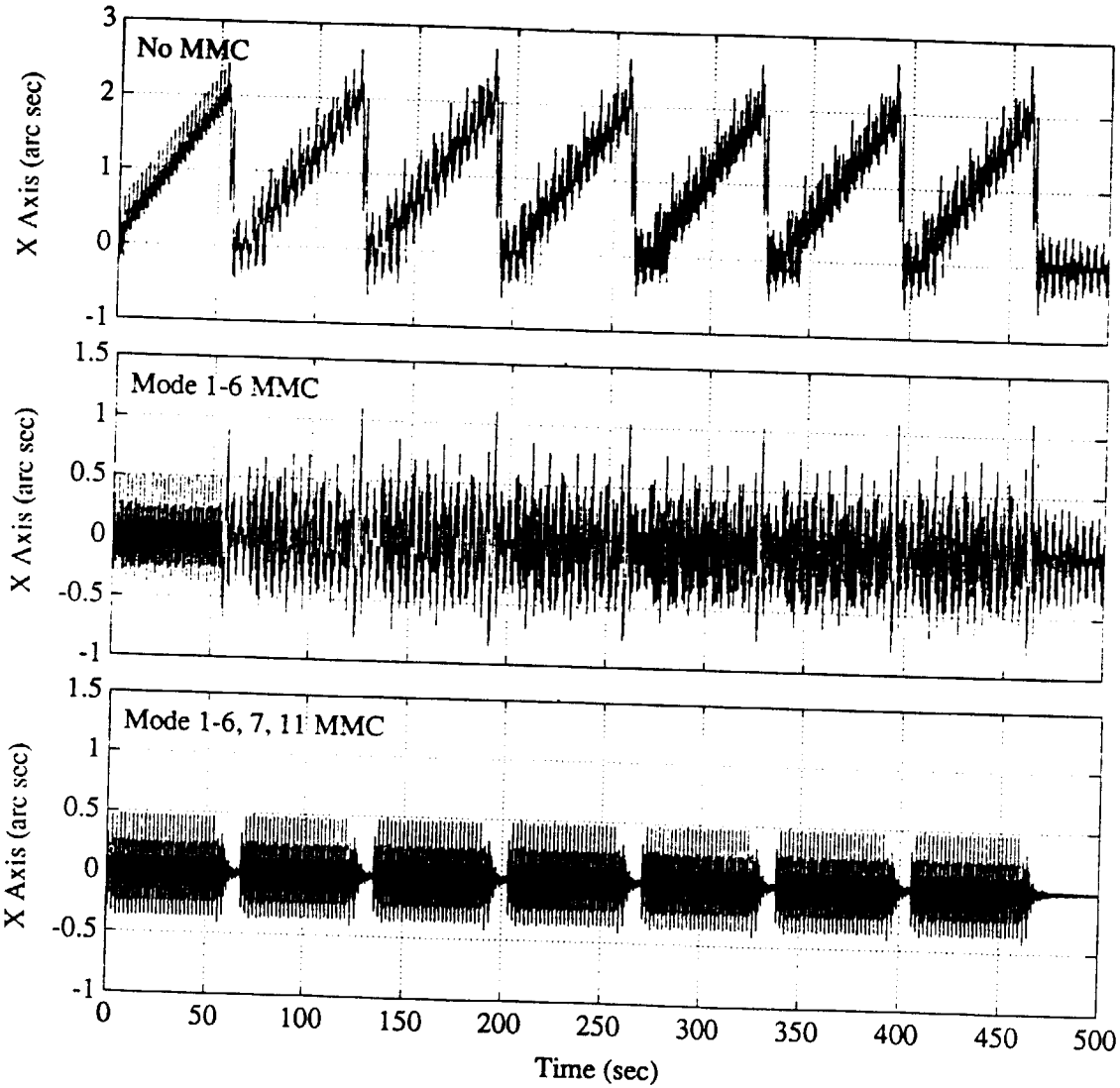

Flexible-Mode Response Equations

The nominal flex-body response is also in four parts. The responses are scaled sinusoids at the damped modal frequency and shifted in phase. These equations substituted into those on slide 10 give the closed-form solution used to evaluate the response curves.

The scale factors are functions of the modal frequency, modal damping, pulse widths, and time span between the two pulses. The equations shown are valid for either a forward or return torque pulse pair, where Ts is replaced by the appropriate Tf or Tr.

The various coefficients introduced in these equations are given on the following page.

Flexible-Mode Response Equations

Response to one forward or return pulse pair

$$x_j(t) = \frac{A}{\omega_j^2 \sin\phi_j} \begin{cases} \sin\phi_j - e^{-\zeta_j \omega_j t} \sin(\omega_{jd} t + \phi_j) & \forall t \varepsilon [0, 2T) \\ \gamma_{1j} e^{-\zeta_j \omega_j t} \sin(\omega_{jd} t + \psi_{1j}) & \forall t \varepsilon [2T, T_s) \\ \gamma_{2j} e^{-\zeta_j \omega_j t} \sin(\omega_{jd} t + \psi_{2j}) - 2\sin\phi_j & \forall t \varepsilon [T_s, T_s + T) \\ \gamma_{3j} e^{-\zeta_j \omega_j t} \sin(\omega_{jd} t + \psi_{3j}) & \forall t \geq T_s + T \end{cases}$$

Flexible-Mode Response Equations (cont.)

These equations define those parameters introduced in the equations on the previous page.

Flexible-Mode Response Equations (cont.)

$$\omega_{jd} = \omega_j \sqrt{1-\zeta_j^2}, \qquad \phi_j = \tan^{-1}\left[\frac{\sqrt{1-\zeta_j^2}}{\zeta_j}\right]$$

$$\gamma_{1j} = \sqrt{\left[e^{2\zeta_j\omega_j T}\sin\left(\phi_j - 2\omega_{jd}T\right) - \sin\phi_j\right]^2 + \left[e^{2\zeta_j\omega_j T}\cos\left(\phi_j - 2\omega_{jd}T\right) - \cos\phi_j\right]^2}$$

$$\gamma_{2j} = \sqrt{\left[\gamma_{1j}\sin\psi_{1j} + 2e^{\zeta_j\omega_j T_s}\sin\left(\phi_j - \omega_{jd}T_s\right)\right]^2 + \left[\gamma_{1j}\cos\psi_{1j} + 2e^{\zeta_j\omega_j T_s}\cos\left(\phi_j - \omega_{jd}T_s\right)\right]^2}$$

$$\gamma_{3j} = \sqrt{\left[\gamma_{1j}\sin\psi_{1j} - 2\xi_{2j}e^{\zeta_j\omega_j T_s}\sin\left(\varphi_{2j} - \omega_{jd}T_s\right)\right]^2 + \left[\gamma_{1j}\cos\psi_{1j} - 2\xi_{2j}e^{\zeta_j\omega_j T_s}\cos\left(\varphi_{2j} - \omega_{jd}T_s\right)\right]^2}$$

$$\psi_{1j} = \tan^{-1}\left[\frac{e^{2\zeta_j\omega_j T}\sin\left(\phi_j - 2\omega_{jd}T\right) - \sin\phi_j}{e^{2\zeta_j\omega_j T}\cos\left(\phi_j - 2\omega_{jd}T\right) - \cos\phi_j}\right]$$

$$\psi_{2j} = \tan^{-1}\left[\frac{\gamma_{1j}\sin\psi_{1j} + 2e^{\zeta_j\omega_j T_s}\sin\left(\phi_j - \omega_{jd}T_s\right)}{\gamma_{1j}\cos\psi_{1j} + 2e^{\zeta_j\omega_j T_s}\cos\left(\phi_j - \omega_{jd}T_s\right)}\right]$$

$$\psi_{3j} = \tan^{-1}\left[\frac{\gamma_{1j}\sin\psi_{1j} - 2\xi_{2j}e^{\zeta_j\omega_j T_s}\sin\left(\varphi_{2j} - \omega_{jd}T_s\right)}{\gamma_{1j}\cos\psi_{1j} - 2\xi_{2j}e^{\zeta_j\omega_j T_s}\cos\left(\varphi_{2j} - \omega_{jd}T_s\right)}\right]$$

$$\xi_{2j} = \sqrt{\left[e^{\zeta_j\omega_j T}\sin\left(\phi_j - \omega_{jd}T\right) - \sin\phi_j\right]^2 + \left[e^{\zeta_j\omega_j T}\cos\left(\phi_j - \omega_{jd}T\right) - \cos\phi_j\right]^2}$$

$$\varphi_{2j} = \tan^{-1}\left[\frac{e^{\zeta_j\omega_j T}\sin\left(\phi_j - \omega_{jd}T\right) - \sin\phi_j}{e^{\zeta_j\omega_j T}\cos\left(\phi_j - \omega_{jd}T\right) - \cos\phi_j}\right]$$

Pointing Error with Gimbal Noise

These plots show the effect of zero mean, 3 microradian (3σ) gimbal noise on the baseline pointing error, the residual pointing error after rigid-body MMC, and the residual pointing error after rigid-body and mode 7 and 11 MMC. The combined effect of the stochastic gimbal noise and deterministic disturbance response is additive.

The flexible-mode MMC has not reduced the pointing error as much as when there was no gimbal noise since the gimbal noise and the baseline post-flex-mode MMC residuals have approximately the same magnitude. However, there is still a significant improvement.

Note that the lower two plots have a half the scale of the top plot.

Pointing Error with Gimbal Noise

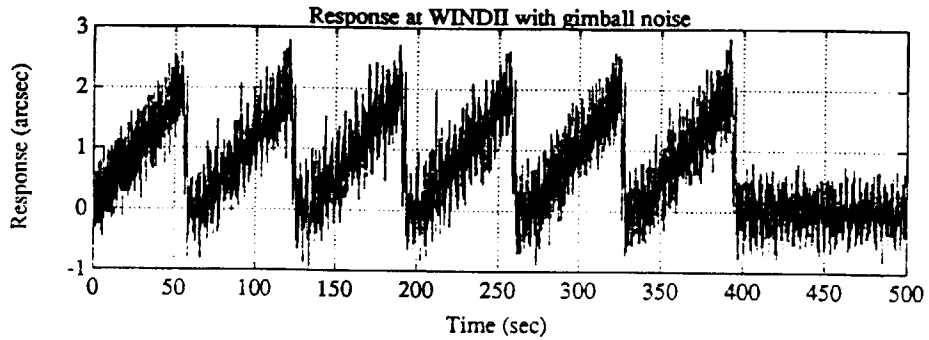

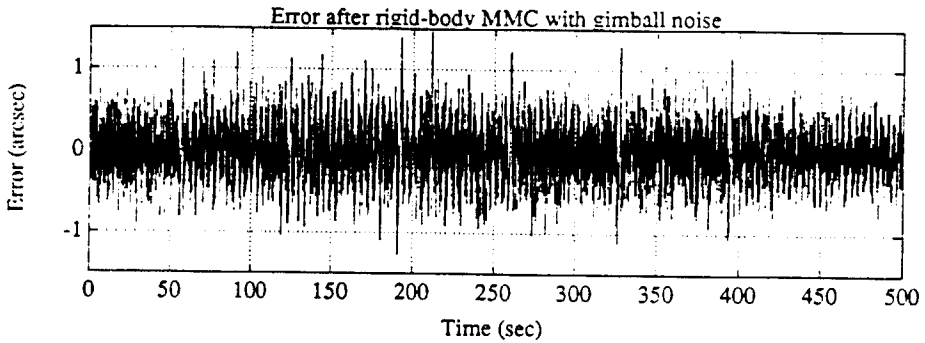

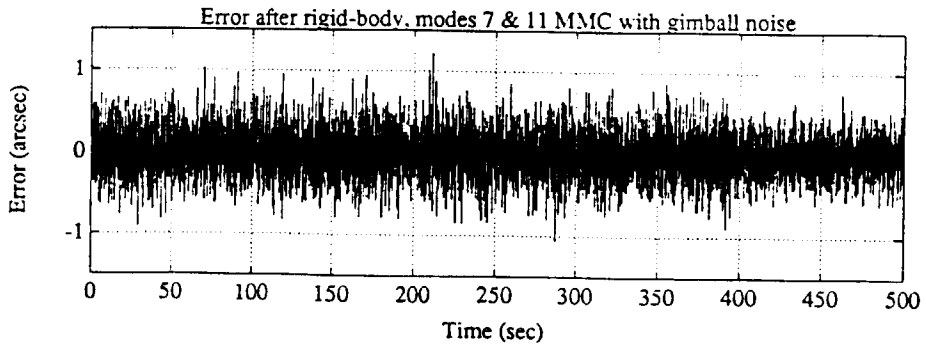

Gimbal noise:

3 μrad (3σ) white

Mode 7 MMC - Effect of Frequency Error

The top plot shows the response of mode 7, the lowest frequency flexible mode (solar array out of plane 1st bending mode), at WINDII to the MLS scan 3 torque pulse sequence. Note that this modal response contains the large spike responses to the 2 impulsive return pulses that can be seen in the full system response at WINDII in slide 21. The response of mode 7 is almost entirely due to the excitation from the return pulses. The forward pulses do not significantly affect the response after the return pulses.

The next 3 plots show the residual error after MMC when the compensation is at an incorrect frequency, for frequency errors of +10%, +1% and +0.1% respectively. This shows that relatively small frequency errors have a significant impact on the RMS error, and that the compensation frequency must be very close to the actual modal frequency for significant reductions in the residual MMC RMS error.

Note that the error amplitude is modulated by the frequency difference, which illustrates the expected "beating" between the response and compensation. The beat period increases as the frequency error decreases.

The elimination of the responses due to the impulsive return pulses is not affected by the frequency error. A frequency error in the compensation causes an eventual build-up of phase error that is the root of the residual MMC error, but has little impact over the initial residual error to a specific disturbing event whos timing is known (where "short term" implies much shorter than the period of the frequency error).

Mode 7 MMC - Effect of Frequency Error

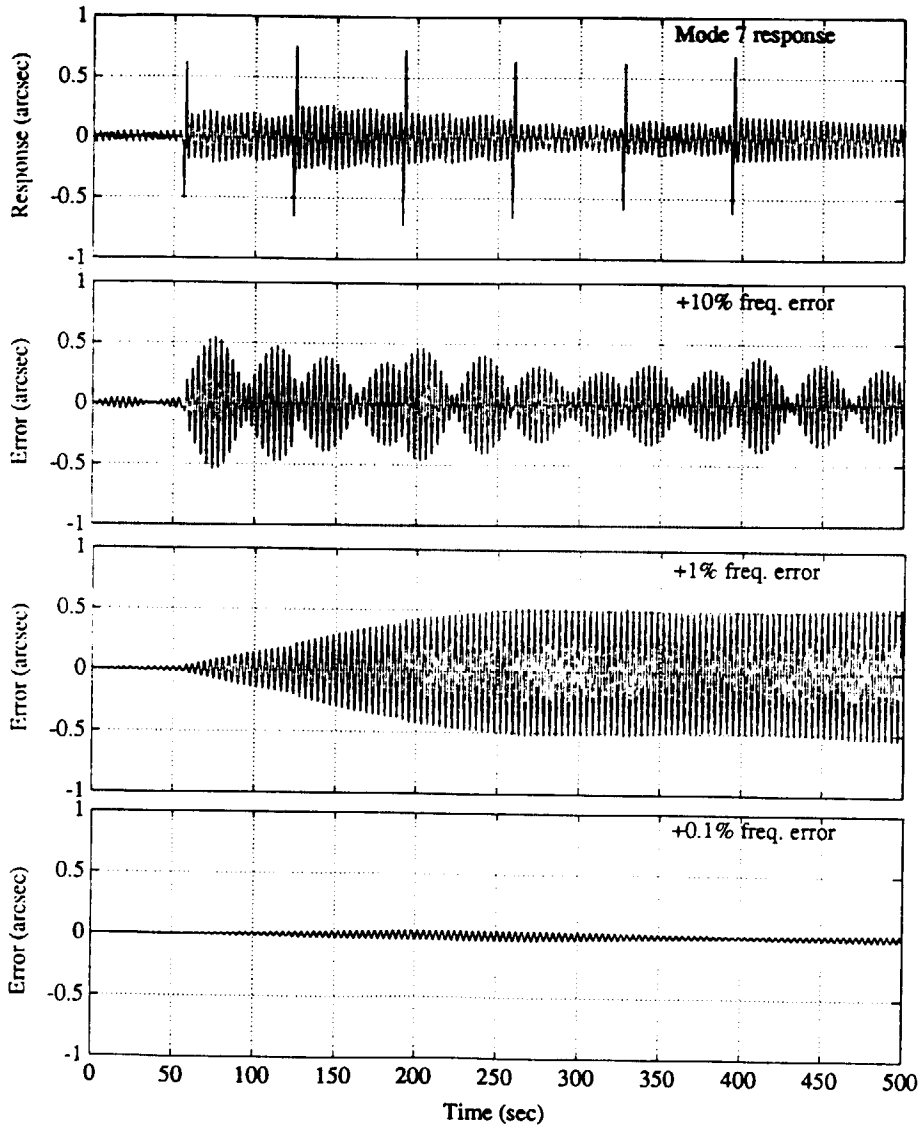

Mode 11 MMC - Effect of Frequency Error

This sequence of plots is similar to that given on the previous slide, but now for flexible mode 11. The same trends can be seen indicating the extreme sensitivity of the MMC error to the frequency error in the modal compensation.

Note that the response of mode 11 is again almost entirely due to the excitation from the return pulses. The forward pulses do not significantly affect the decay of the response after the return pulses.

The response of mode 11 looks quite different from that of mode 7. This is due to the different excitations to each flex mode from the specific shape and timing of the scan profile.

Mode 11 MMC - Effect of Frequency Error

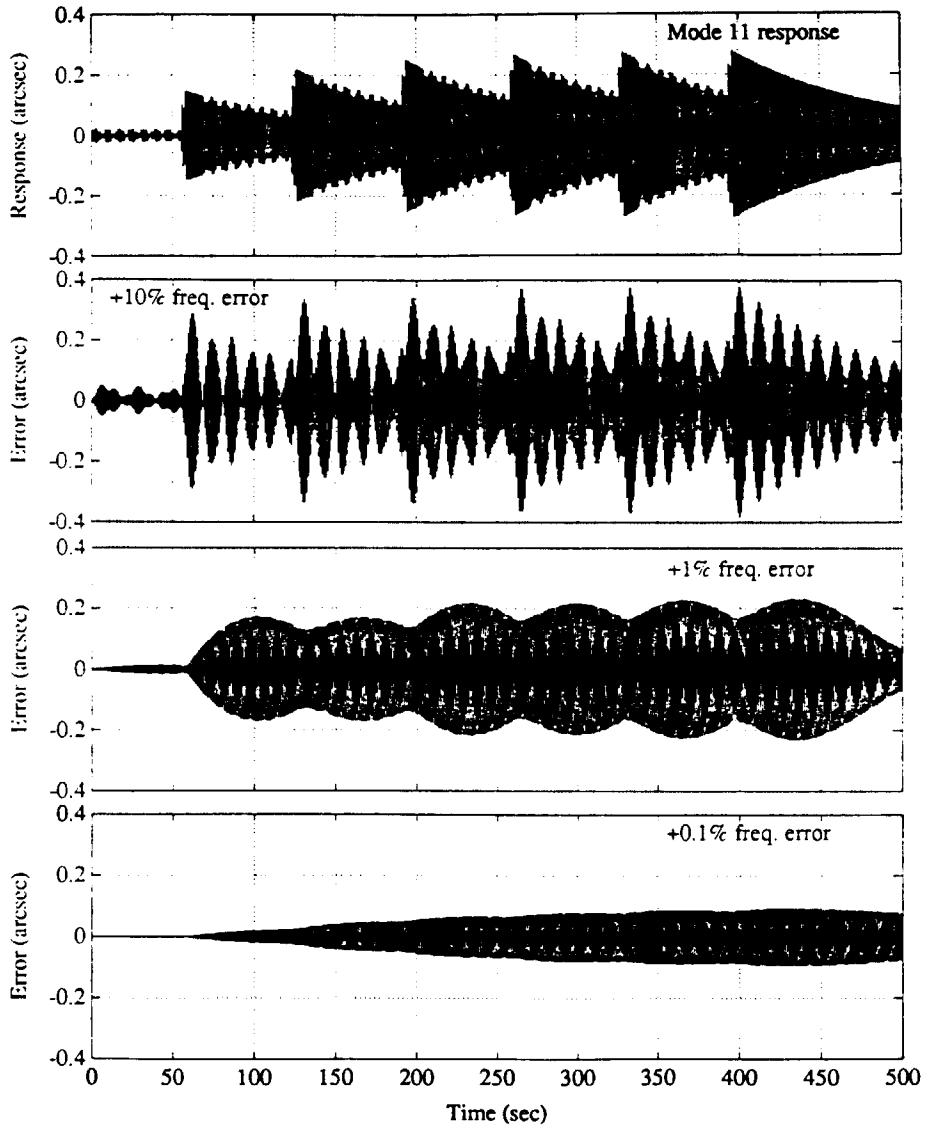

MMC with 10% Frequency Mismatch on Both Modes

These plots show the effect of MMC frequency errors on the MMC performance over the rigid-body MMC performance (where, of course, there can be no frequency error). The top plot gives the residual error after rigid-body MMC, and the bottom plot gives the residual error after the addition of mode 7 and 11 MMC with +10% frequency errors on both modal compensations.

The frequency errors in the compensation have a very significant impact on the ability of the MMC to reduce the pointing error due to flexible mode excitation. In fact, no significant reduction in pointing error was obtained with 10% frequency errors in the compensation. If the peak responses at the return pulse times are ignored, the MMC actually increases the errors at WINDII due to the disturbances at MLS.

MMC with 10% Frequency Mismatch on Both Modes

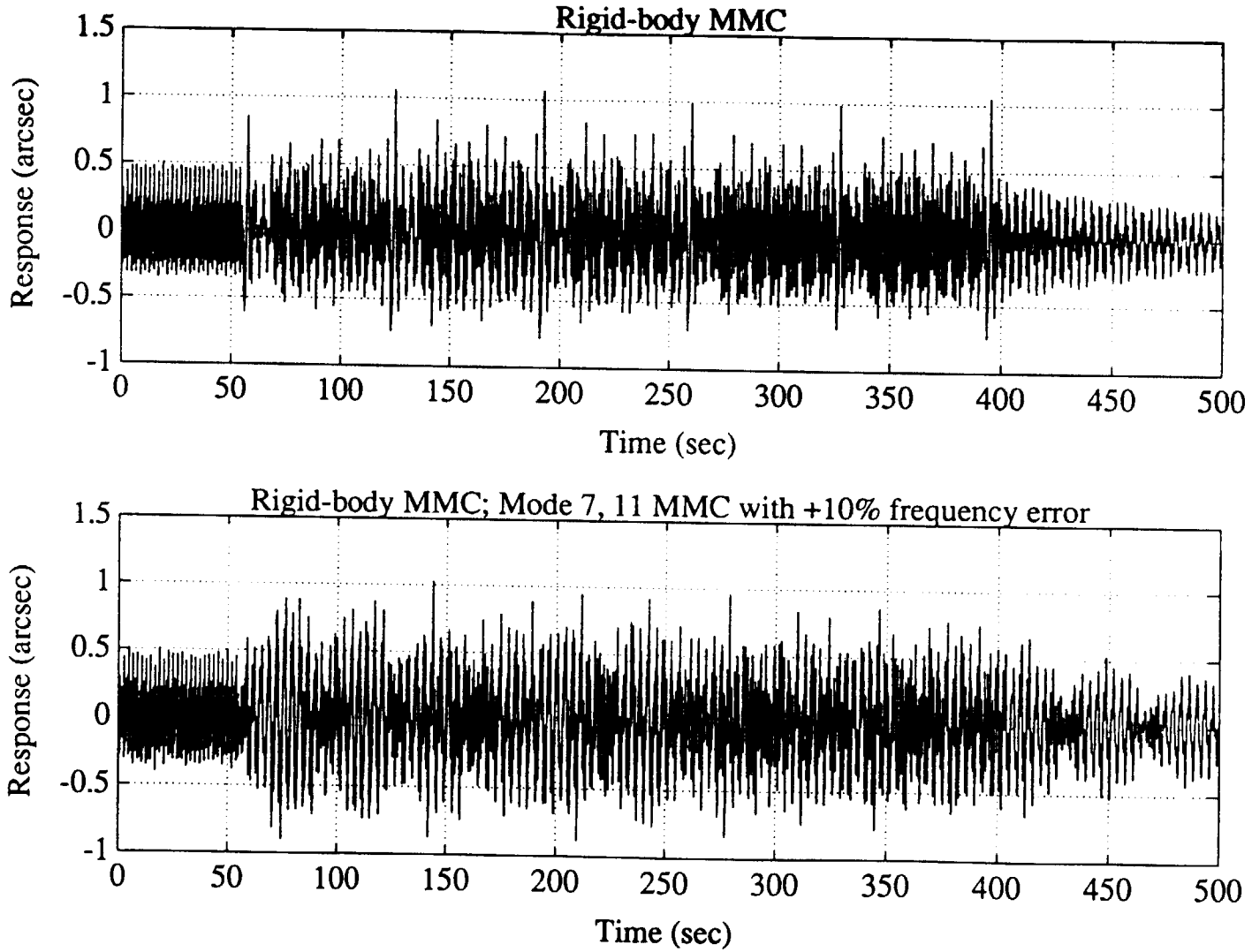

Effect of Modal Frequency Uncertainty

The effect of modal frequency errors on the flexible-mode MMC performance can be investigated analytically by considering the difference of two sinusoids with differing frequencies and phases. The result is a sinusoid with a frequency and phase that are the averaged values of the two signals, and a time varying amplitude and phase that exhibit a "beating" phenomenon.

This amplitude has a maximum that is generally at the point of maximum in the first beat cycle. This maximum can be approximated, and is a function of the frequency error, modal damping, and phase difference. A plot of this maximum amplitude function is given on the next slide.

Effect of Frequency Uncertainty

Residual error of difference of two sinusoids of differing frequency and phase:

$$= e^{-\zeta\omega t}\sin\left(\sqrt{1-\zeta^2}\,\omega t+\psi\right)-e^{-\zeta(\omega+\Delta\omega)t}\sin\left(\sqrt{1-\zeta^2}\,(\omega+\Delta\omega)t+(\psi+\Delta\psi)\right)$$

$$= \Gamma e^{-\zeta(\omega+\Delta\omega/2)t}\sin\left(\sqrt{1-\zeta^2}\,(\omega+\Delta\omega/2)t+(\psi+\Delta\psi/2)+\Phi\right)$$

Magnitude of residual is:

$$\Gamma = 2\left[\sinh^2(\zeta\Delta\omega/2)+\sin^2\left[\tfrac{1}{2}\left(\sqrt{1-\zeta^2}\,\Delta\omega t+\Delta\psi\right)\right]\right]^{\frac{1}{2}}$$

which has a maximum:

$$\Gamma(t_m)\approx 2e^{-\zeta\Delta\omega t_m/2}\cosh(\zeta\Delta\omega t_m/2) \quad \text{at} \quad t_m=\frac{(2n+1)\pi/2-\Delta\psi}{\sqrt{1-\zeta^2}\,\Delta\omega}$$

Sensitivity of MMC Error to Frequency Uncertainty

The maximum value of the time varying amplitude from the previous slide is shown here normalized to the nominal amplitude and plotted against the normalized frequency difference of the subtracted sinusoid. The different curves represent different damping ratios. The MMC approach of subtracting the estimated modal response would only be helpful if the normalized error amplitude is less than 1 (the break even point). Note that this is only the case for very small frequency errors.

Since the entire error envelope is decaying at the modal damping rate, increasing modal damping has the effect of reducing the maximum value the beating sinusoid will attain. This gives the characteristic dip in the curve for small frequency changes and large damping.

These curves show that the frequency of the modal compensation must be very close to the actual modal frequency for the compensation to be of any use at all for typical values of the modal damping. For damping of 0.002 (a typical conservative design point), the compensation frequency must be within approximately 0.5% of the actual modal frequency for the maximum error after compensation to be smaller than the initial modal response. For a significant reduction in pointing error, the compensation frequency must be much closer to the actual modal frequency than that.

In the current example of WINDII errors due to MLS disturbances, the peak flexible-mode responses due to the return pulses are still eliminated by flexible-mode MMC regardless of frequency errors. Hence, even a break-even point for the flexible-mode MMC will reduce the error over that apparent with just rigid-body MMC applied. For typical on-orbit observed solar array damping of 1%, the solar array fundamental mode frequency should therefore be known to within about 2%.

Sensitivity of MMC Error to Frequency Uncertainty

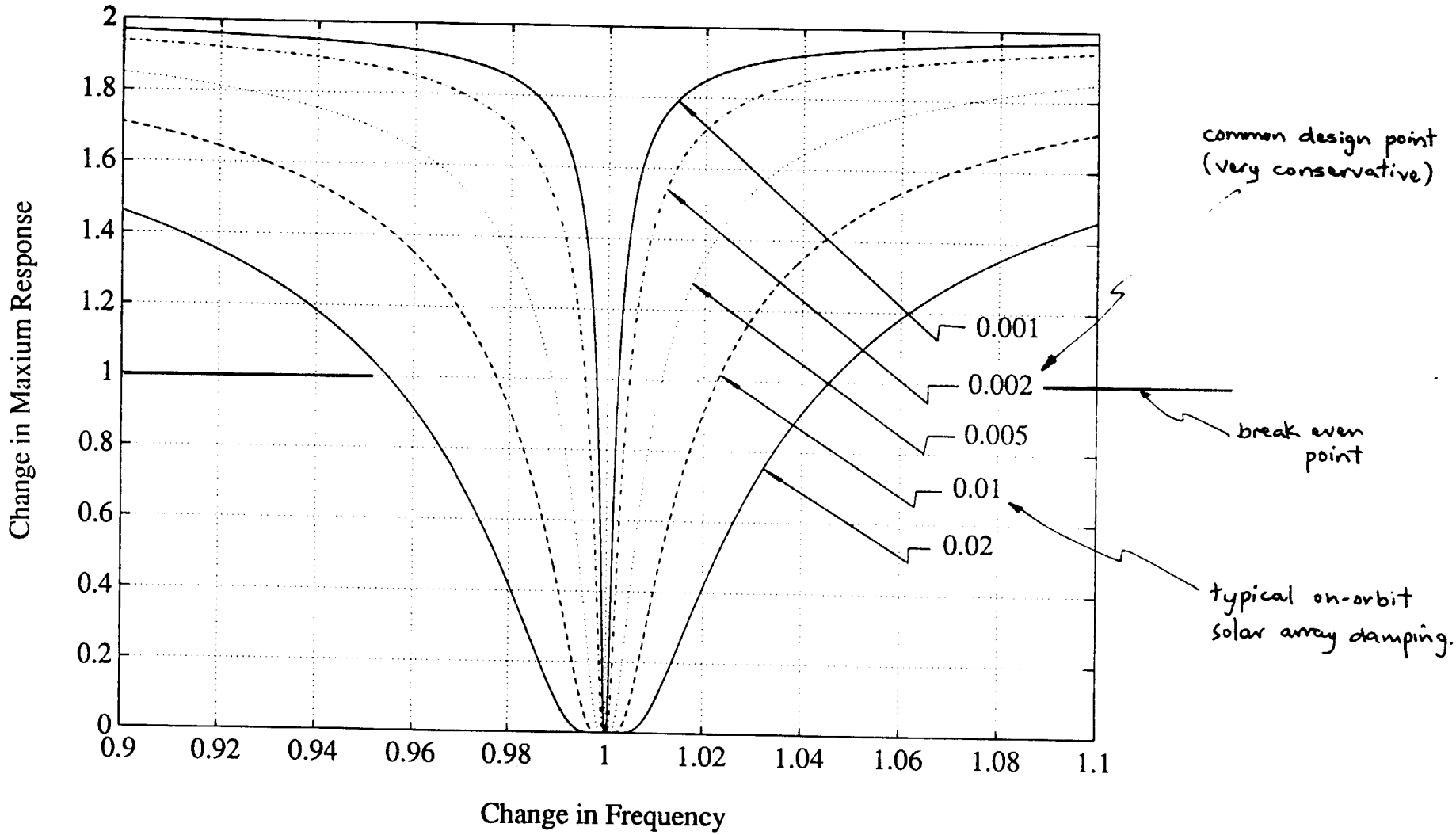

Equations for MMC with Frequency Errors

For the WINDII response to the MLS scan pulse sequences, the amplitudes are functions of the modal frequency. By subtracting the appropriate magnitude, frequency, and phase shifted compensation signals from the UARS flexible-body response equations, analytical expressions can be developed for the MMC residual errors due to a modal frequency error.

The equations shown are in four parts, corresponding to the four parts of the modal response equations given earlier. These equations are valid for both the forward and return torque pulse pairs, provided the appropriate pulse timings Tf and Tr respectively are used for Ts to evaluate the parameters.

These equations give a theoretical validation to the results seen in the simulations. The magnitudes and phase shifts due to the MMC frequency error are sinusiodal at the beat frequency.

Equations for MMC with Frequency Errors

$$x_j(t) = \frac{A}{\omega_j^2 \sin\phi_j} \begin{cases} 2\left(\frac{\Delta\omega_j}{\omega_j}\right)\sin\phi_j + \Gamma_j e^{-\zeta_j\omega_j t}\sin(\omega_{jd}t + \phi_j + \Phi_j) & \forall t\varepsilon[0,2T) \\ \Gamma_{1j}\gamma_{1j}e^{-\zeta_j\omega_j t}\sin(\omega_{jd}t + \psi_{1j} - \Psi_{1j}) & \forall t\varepsilon[2T,T_s) \\ \Gamma_{2j}\gamma_{2j}e^{-\zeta_j\omega_j t}\sin(\omega_{jd}t + \psi_{2j} - \Psi_{2j}) - 2\sin\phi_j & \forall t\varepsilon[T_s,T_s+T) \\ \Gamma_{3j}\gamma_{3j}e^{-\zeta_j\omega_j t}\sin(\omega_{jd}t + \psi_{3j} - \Psi_{3j}) & \forall t \geq T_s + T \end{cases}$$

where:

$$\Gamma_j = \sqrt{\left[\beta e^{-\zeta_j\omega_j t}\cos\left(\Delta\omega_{jd}t\right) - 1\right]^2 + \left[\beta e^{-\zeta_j\omega_j t}\sin\left(\Delta\omega_{jd}t\right)\right]^2}$$

$$\Gamma_{kj} = \sqrt{\left[1 - \alpha_{kj}\beta e^{-\zeta_j\omega_j t}\cos\left(\Delta\omega_{jd}t + \Delta\psi_{kj}\right)\right]^2 + \left[\alpha_{kj}\beta e^{-\zeta_j\omega_j t}\sin\left(\Delta\omega_{jd}t + \Delta\psi_{kj}\right)\right]^2}$$

$$\phi_j = \tan^{-1}\left[\frac{\beta e^{-\zeta_j\omega_j t}\sin\left(\Delta\omega_{jd}t\right)}{\beta e^{-\zeta_j\omega_j t}\cos\left(\Delta\omega_{jd}t\right) - 1}\right], \qquad \Psi_{kj} = \tan^{-1}\left[\frac{\alpha_{kj}\beta e^{-\zeta_j\omega_j t}\sin\left(\Delta\omega_{jd}t + \Delta\psi_{kj}\right)}{1 - \alpha_{kj}\beta e^{-\zeta_j\omega_j t}\cos\left(\Delta\omega_{jd}t + \Delta\psi_{kj}\right)}\right]$$

$$\alpha_{kj} = \left[1 + \left(\frac{\Delta\gamma_{kj}}{\gamma_{kj}}\right)\right], \qquad \beta = 1 - 2\left(\frac{\Delta\omega_j}{\omega_j}\right)$$

Mode 7 - Effect of Modal Damping Error

The top plot shows the response of mode 7, the lowest frequency flexible mode (solar array 1st out of plane bending mode), at WINDII to the MLS scan 3 torque pulse cycles.

The next 3 plots show the residual error after MMC when the modal compensation has incorrect damping, while all other model parameters are assumed known exactly. The compensation damping here is assumed to be constant at 0.2%, while the actual modal damping is 0.1%, 0.5%, and 1% respectively for the 3 plots. The errors here seem quite small, so that there is still a benefit to be gained in MMC for mode 7 even with damping uncertainties.

The large spikes in the mode 7 response due to the impulsive return pulse excitation can be seen to be fully compensated, and do not appear in the residual modal error. This is because an error in the compensation damping causes a slow build-up of phase error that eventually becomes large if the damping is low enough. However, the compensation of impulsive disturbances is not affected.

Mode 7 - Effect of Modal Damping Error

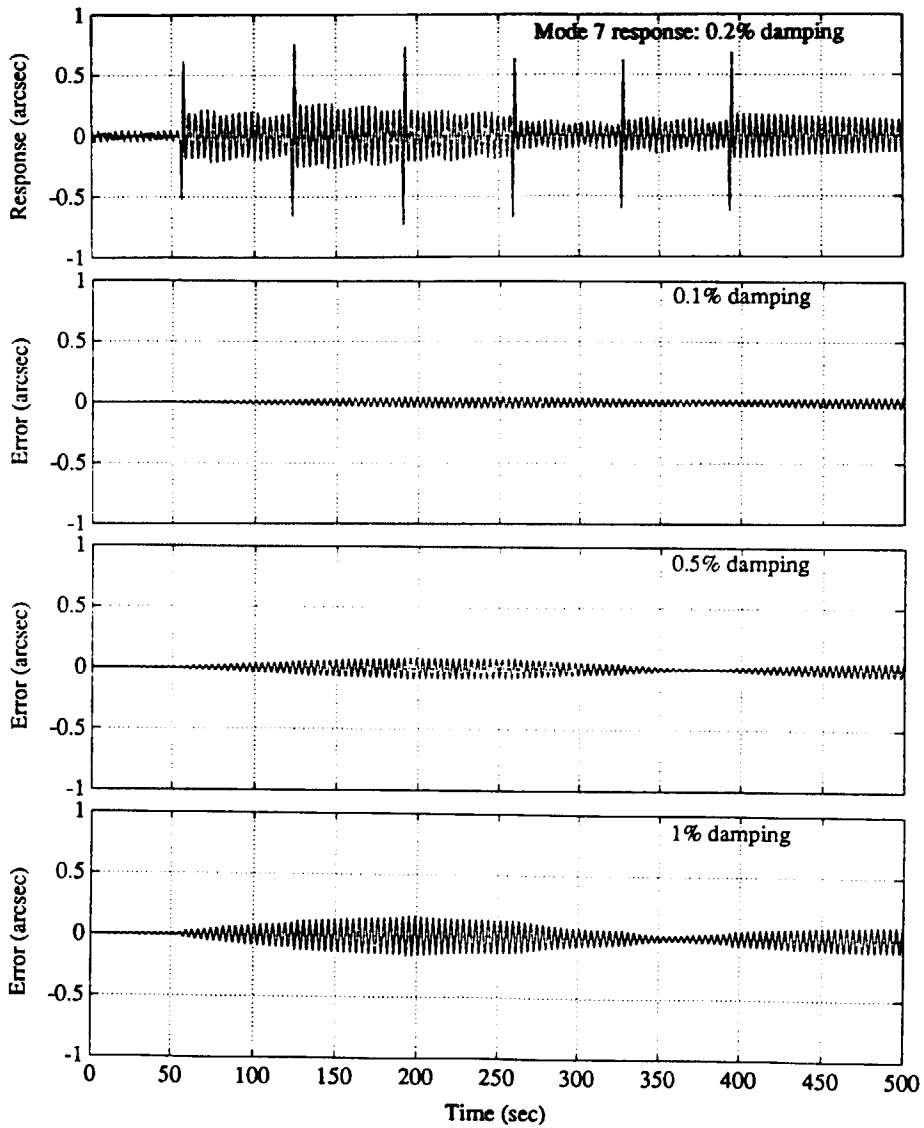

Mode 11 - Effect of Modal Damping Error

The top plot shows the response of mode 11 (the ZEPS boom fundamental mode) at WINDII to the MLS scan 3 torque pulse cylces.

The next 3 plots show the residual error after MMC when the compensation has an incorrect damping. The compensation damping here is assumed to be constant at 0.2%, while the actual modal damping is 0.1%, 0.5%, and 1% respectively for the 3 plots. The same damping error for mode 11 gives a faster phase build-up, which leads to poorer results for mode 11 than were obtained for mode 7 on the previous page. However, the error due to mode 11 MMC is still small enough in comparison to the mode 11 response that mode 11 MMC seems worthwhile.

Mode 11 - Effect of Modal Damping Error

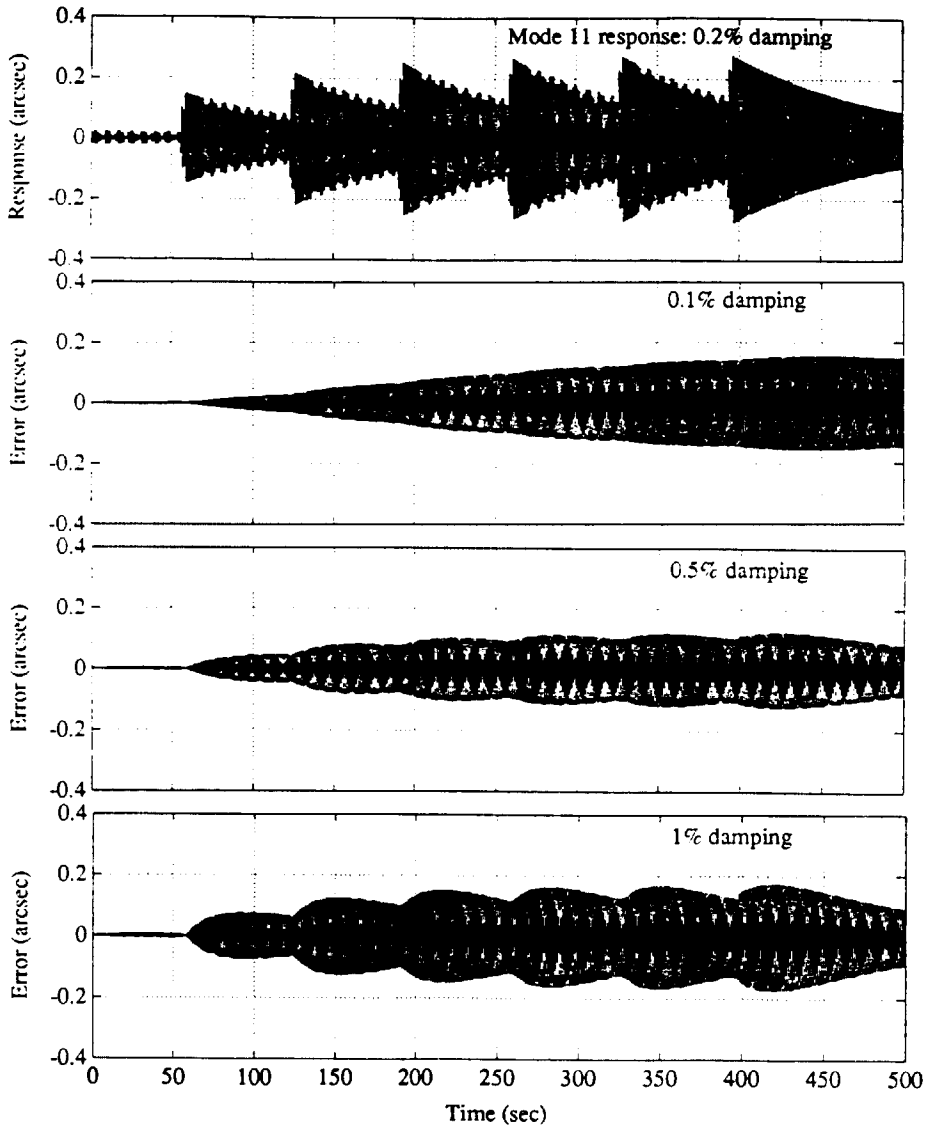

MMC with Modal Damping Errors

These plots show the effect of MMC damping errors on the MMC performance over the rigid-body MMC performance (where, of course, there can be no damping error). The top plot gives the residual error after rigid-body MMC, and the bottom plot gives the residual error after the addition of mode 7 and 11 MMC where the modal damping is 1% but the compensation has 0.2% damping.

It can be seen that although there is some degradation over the case where perfect damping information was obtained, there is still a significant benefit to the mode 7 and 11 MMC. In particular, the large spikes at the return pulse times due to mode 7 and 11 excitations are much reduced.

MMC with Modal Damping Errors

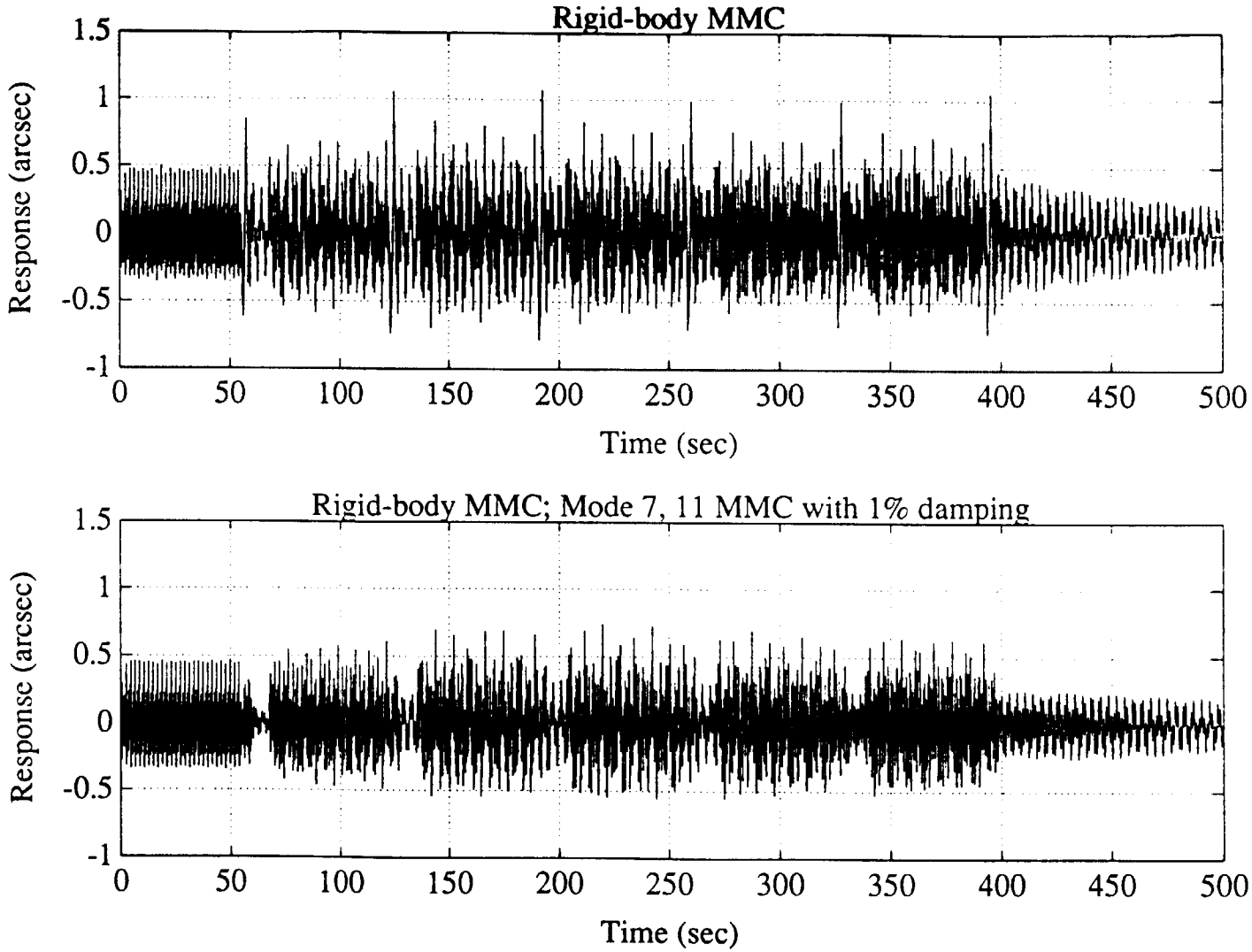

Equations for MMC with Modal Damping Errors

The equations listed here are an approximation for the residual MMC error of one mode to an MMC with a damping error, for "small" modal damping. The damping error causes a change in the frequency and phase of the compensation with respect to the response, which produce an error with time varying magnitude and phase. The time varying component will usually be very slow.

The elimination of peak responses due to the initial modal response to disturbances is unaffected by the damping error. A damping error in the compensation causes an eventual build-up of phase and magnitude error that are the source of the residual MMC error, but has little impact on the initial residual error to a specific impulsive disturbing event.

- If the compensation damping is larger than the actual modal damping, the compensation damps out before the actual response being compensated, and the error becomes simply the response due to excitation in the long term .
- If the actual modal damping is larger than the compensation damping, the response to be compensated damps out before the compensation, and the error becomes the compensation in the long term.. This is illustrated, for example, for the 1% damping case for mode 11.

The error in the long term becomes whichever of the modal response and compensation has the lower damping. If the compensation damping is always larger than the actual modal damping, then the flexible-mode MMC will not increase the pointing error from the pre-MMC level.

Equations for MMC with Damping Errors

$$e_j(t) \approx \frac{Ae^{-\zeta_j \omega_j t}}{\omega_j^2} \begin{cases} (1 + e^{-\zeta_j \omega_j t}) \cos(\omega_{jd} t) & \forall t \varepsilon [0, 2T) \\ \Gamma_{1j} \gamma_{1j} \sin(\omega_{jd} t + \psi_{1j} - \Psi_{1j}) & \forall t \varepsilon [2T, T_s) \\ \Gamma_{2j} \gamma_{2j} \sin(\omega_{jd} t + \psi_{2j} - \Psi_{2j}) & \forall t \varepsilon [T_s, T_s + T) \\ \Gamma_{3j} \gamma_{3j} \sin(\omega_{jd} t + \psi_{3j} - \Psi_{3j}) & \forall t \geq T_s + T \end{cases}$$

where:

$$\Gamma_{ij} = \sqrt{\left[1 - \alpha_{ij} e^{-\Delta\zeta_j \omega_j t} \cos\left(\Delta\psi_{ij} - 2\Delta\zeta_j \omega_j t\right)\right]^2 + \left[\alpha_{ij} e^{-\Delta\zeta_j \omega_j t} \sin\left(\Delta\psi_{ij} - 2\Delta\zeta_j \omega_j t\right)\right]^2}$$

$$\psi_{ij} = \tan^{-1}\left[\frac{\alpha_{ij} e^{-\Delta\zeta_j \omega_j t} \sin\left(\Delta\psi_{ij} - 2\Delta\zeta_j \omega_j t\right)}{1 - \alpha_{ij} e^{-\Delta\zeta_j \omega_j t} \cos\left(\Delta\psi_{ij} - 2\Delta\zeta_j \omega_j t\right)}\right]$$

$$\alpha_{ij} = \left[1 + \left(\frac{\Delta\zeta_{ij}}{\zeta_{ij}}\right)\right]$$

Mode 7 - Effect of Modal Residue Error

The top plot shows the response of mode 7, the lowest frequency flexible mode at WINDII to the MLS scan 3 torque pulse sequence.

The next 3 plots show the residual error after MMC when the compensation has an incorrect modal residue. The compensation residue here is assumed to be scaled with respect to the actual residue by +0.5, +2 and +5 respectively for the 3 plots. The errors are simply scaled versions of the modal response.

This is because the modal residue appears linearly in the response equations. Consider, for example, the case when the compensation modal residue is 2x the actual modal residue. The error due to mode 7 MMC is then the negative of the response due to mode 7, since the MMC is subtracting twice the response from the response to leave -1x the response as the error.

Mode 7 - Effect of Modal Residue Error

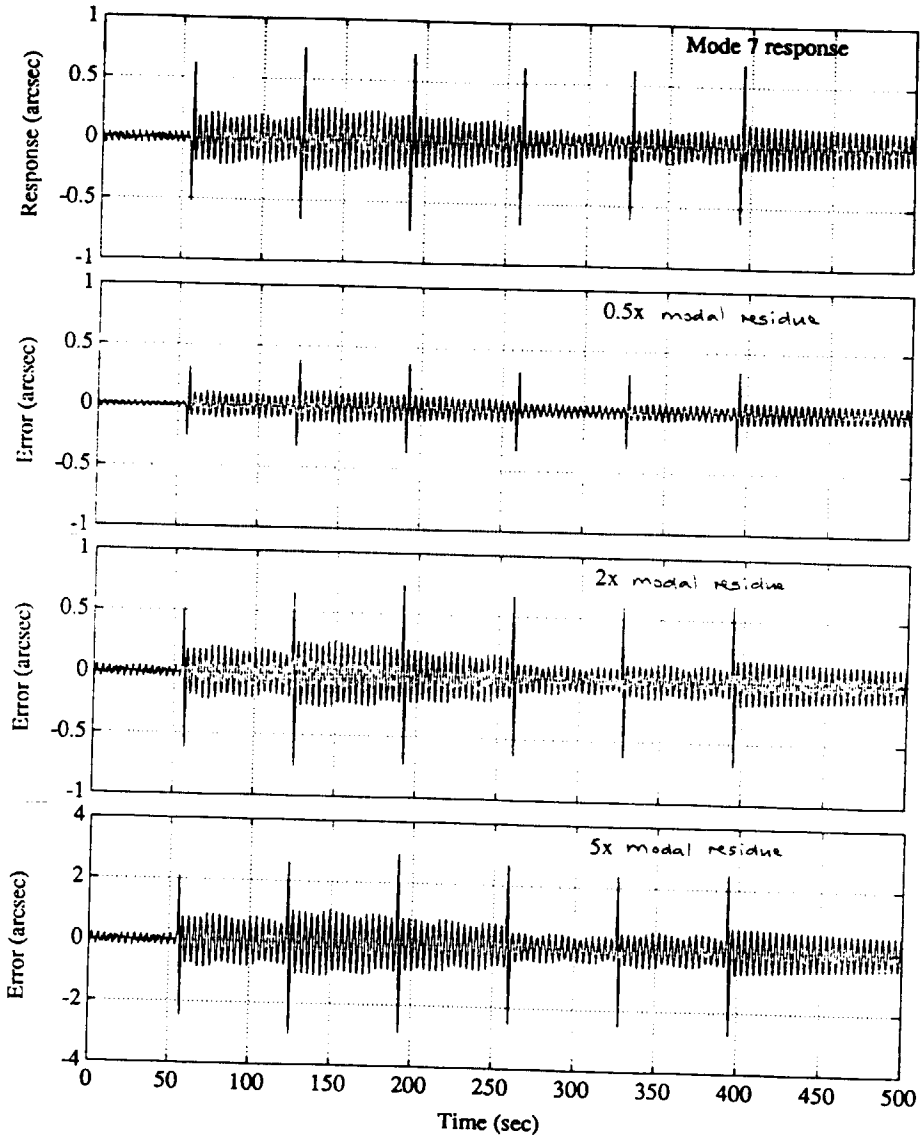

Mode 11 - Effect of Modal Residue Error

This sequence of plots is similar to that given on the previous slide, but now for flexible mode 11. The errors are again scaled versions of the response, as expected.

Mode 11 - Effect of Modal Residue Error

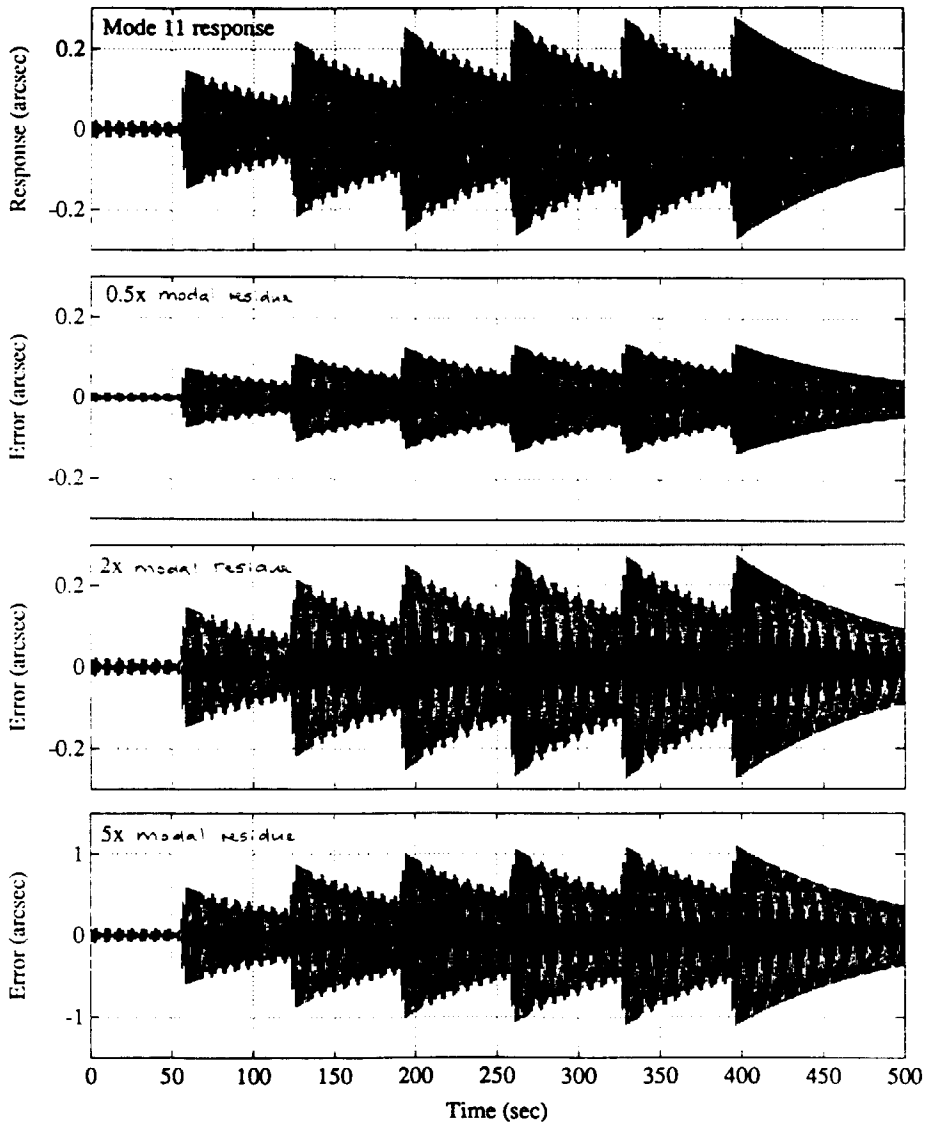

MMC with Modal Residue Errors

These plots show the effect of MMC modal residue errors on the MMC performance over the rigid-body MMC performance. The rigid-body modes are assumed to have no errors in this simulation.

The top plot gives the residual error after rigid-body MMC, and the bottom plot gives the residual error after the addition of mode 7 and 11 MMC where the compensation modal residue corresponding to the MLS disturbance at WINDII has been scaled up by a factor of 2 for both modes. The errors show that no improvement in the pointing error has been obtained by the addition of the two mode MMC if this level of modal residue uncertainty is present.

MMC with Modal Residue Errors

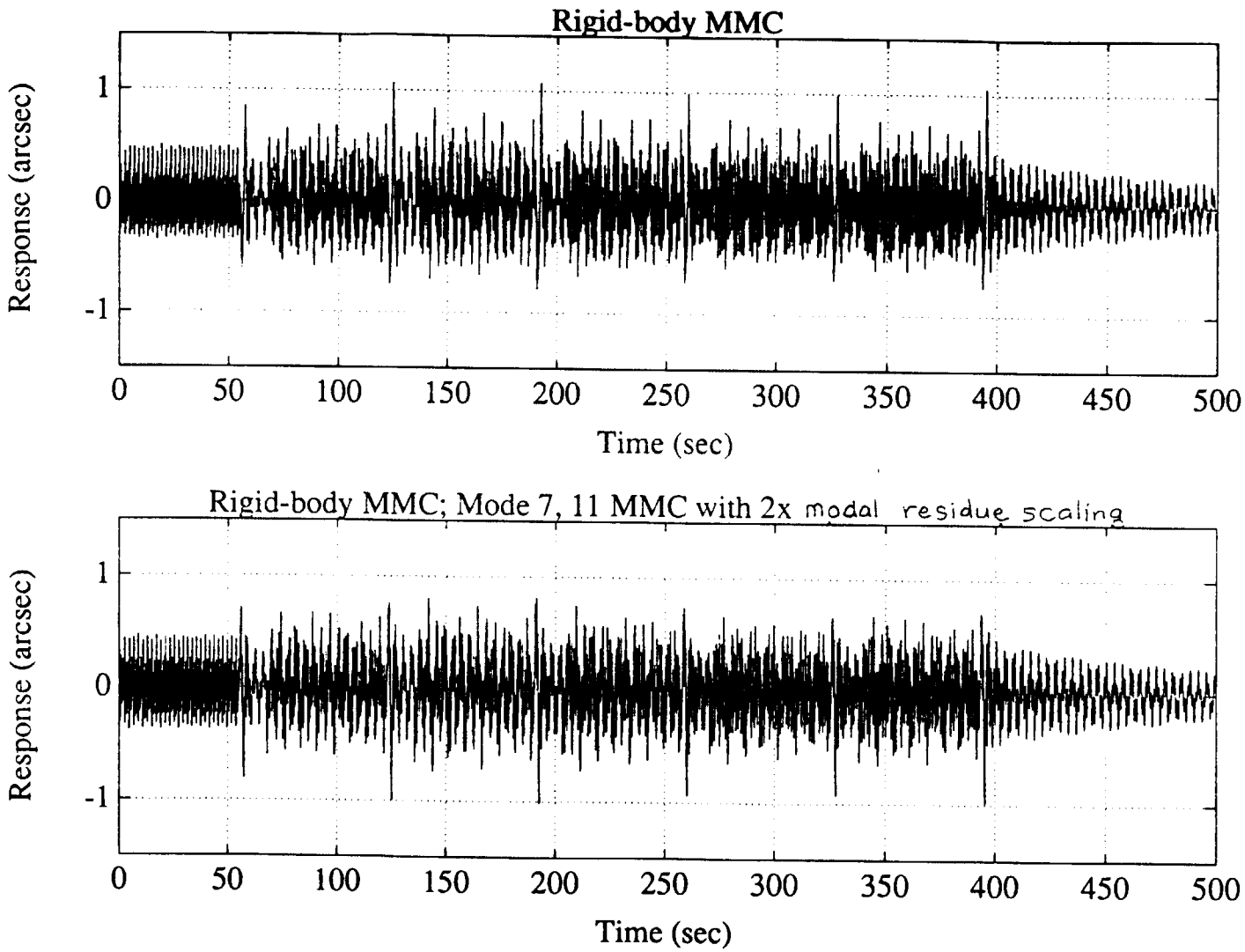

Equations for MMC with Modal Residue Errors

The modal residues appear linearly in the time invariant part of the response equations. The first equation given here is a specific nodal response when the modal residue is scaled. The second equation gives the normalized error after MMC due to the scaling of the compensation residue. The negative sign assumes the scaling is positive.

- If the sign of the compensation residue is the same as that of the actual residue, then the resultant MMC modal error is no more than the actual modal response (the MMC does not increase the pointing error) if the compensation residue is less than twice as large as the actual residue. Otherwise, the error due to MMC is larger than that due to modal response with no MMC.
- If the sign of the compensation residue is different than the actual value, the MMC error will always be larger than the modal response. In this case, MMC will not decrease the pointing error.

For this specific case, modes 7 and 11 are respectively the fundamental modes of vibration for the solar array and ZEPS boom appendages. Therefore, the effect on WINDII from MLS excitation of these appendages is like a rigid-body mode, and the sign of the appropriate modal residue is almost certainly correct.

If the compensation residues are intentionally scaled down to be less than the actual residues, MMC cannot increase the pointing error from that before MMC.

Equations for MMC with Modal Residue Errors

Effect of different compensation and actual modal residues:

$$y_\ell(t)+\Delta y_\ell(t)=\sum_{j=1}^{m}\left[\left(p_{ij}p_{j\ell}\right)+\Delta\left(p_{ij}p_{j\ell}\right)\right]\left[\sum_{k=1}^{n_f}x_{j_f}(t-t_k)+\sum_{k=n_f+1}^{n_f+n_r}x_{j_r}(t-t_k)\right]$$

For the response
of one mode only:

$$\frac{\Delta y_\ell(t)}{y_\ell(t)}=\frac{\Delta\left(p_{ij}p_{j\ell}\right)}{\left(p_{ij}p_{j\ell}\right)}=1-\left(\frac{\text{compensation}\left(p_{ij}p_{j\ell}\right)}{\text{actual}\left(p_{ij}p_{j\ell}\right)}\right)$$

Effect of System Inertia Errors

Uncertainties in the values of the spacecraft and payload inertias correspond into uncertainties in the rigid-body modal residues. However, these inertias are usually known to much better precision than the flexible mode residues.

The effect of errors in the rigid-body residues is again linear. The first plot shown here is the response with no MMC. The second plot is the residual response after the rigid-body MMC assuming perfect rigid-body residue knowledge. The third plot shows the residual response after rigid-body MMC where the compensation rigid-body residues are assumed to be 90% of the actual rigid-body residues (a 10% error in the knowledge of the system inertias).

The effect of the inertia errors is to leave a residual secular component in the pointing error that is proportional to the inertia error percentage. Therefore, a 10% inertia error will result in a rigid-body MMC error that is 10% of the nominal rigid-body response, or about 0.2 arcsec at the end of the scan cycle in this case.

For GOES, with a momentum bias control system, system inertia errors translate into nutation frequency errors. It was well known that knowledge of the nutation frequency was required within very tight tolerances for rigid-body MMC to be effective. This is analogous to the results obtained in this study for errors in the modal frequency. For UARS, with an almost zero-momentum bias control system, there is no significant nutation, and this problem is not apparent. Only the effect shown here concerning the residual rigid-body "drift" will be seen.

Effect of System Inertia Errors

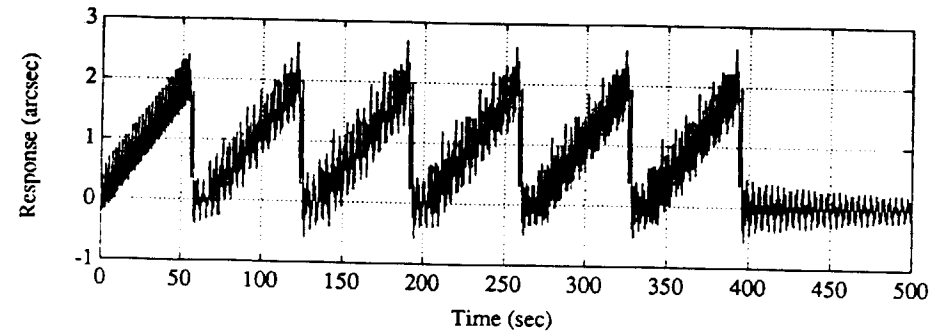

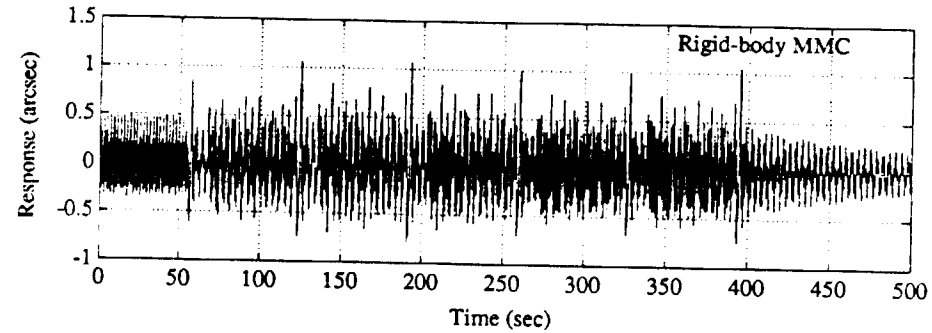

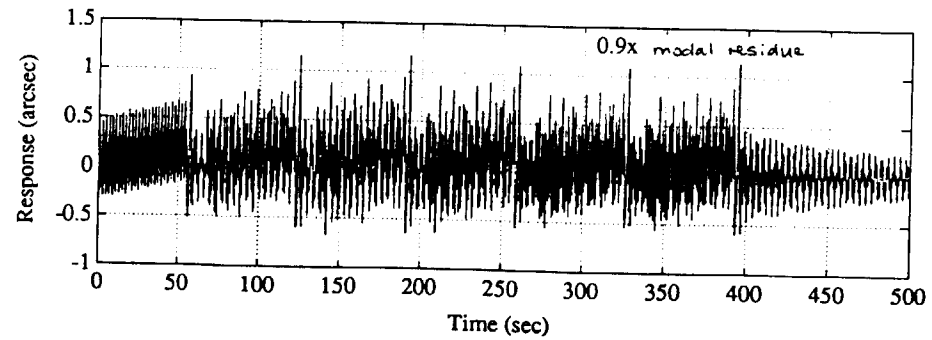

System time delays are introduced into all compensation control systems due to the finite time span taken by any computational operations required to calculate the compensation signals, along with actuator time delay after the command has been received. Additionally the digital nature of most control systems requires that signals can only be applied at discrete time points.

For this study, the time delay is assumed to be 0.2 sec, which is larger than the time span of the forward torque pulse pair (0.078 seconds), but smaller than the time of the start of the second torque pulse in the MLS scan 3 return torque pulse pair (0.737 seconds).

UARS MMC System Time Delay

Time delays in compensation cause associated modal phase errors.

Time delays are present in most systems due to:

- Finite time required to compute the compensation signal
- Digital control system implementation
- Actuator time delay

Rigid-Body - Effect of MMC Time Delay

This plot shows the rigid-body response of WINDII to MLS scan 3 pulse cycles along with the residual rigid-body error due to a 0.2 second time delay.

There are small positive error pulses due to the forward torque pulse pairs, and larger negative pulses due to the return torque pulse pairs. The magnitude of the error pulse due to the forward torque pulse pair is independent of the time delay since the delay is longer than the pulse pair span. The magnitude of the error pulse due to the return torque pulse pair is proportional to the time delay, since the compensation begins while the MLS instrument is still in the coasting phase of its motion. The error is therefore approximately the torque induced rate times the time delay.

Rigid-Body - Effect of MMC Time Delay

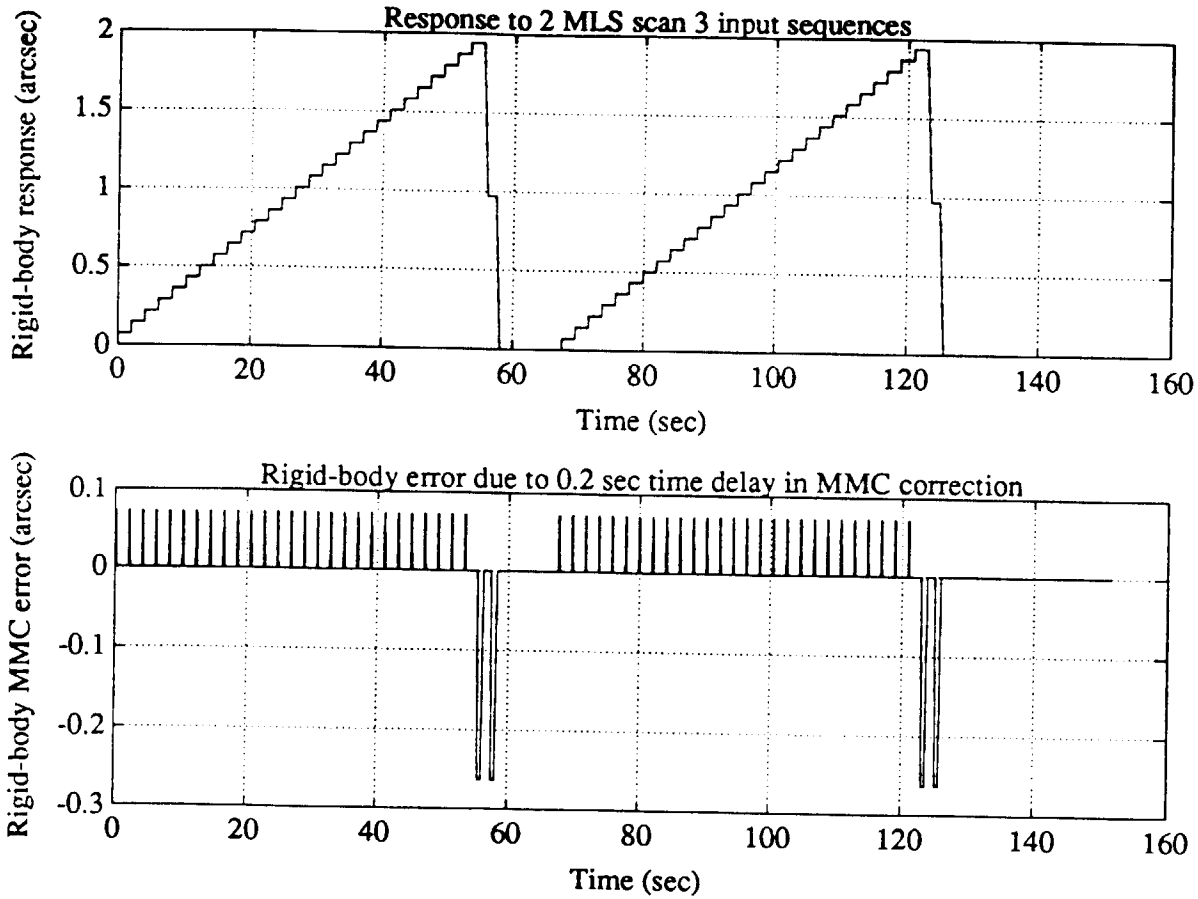

Mode 7 - Effect of MMC Time Delay

This plot shows the response of mode 7 of the UARS model at WINDII due to MLS scan 3 pulse sequences, and the residual error due to mode 7 MMC with a 0.2 second time delay.

For this mode, the MMC approach still results in a reduction in the error magnitude with this time delay. The residual error is due to the compensation phase error for the specific time delay. In this case, the time delay causes only a small phase shift in the compensation sinusoid, hence the error is small.

Mode 7 - Effect of MMC Time Delay

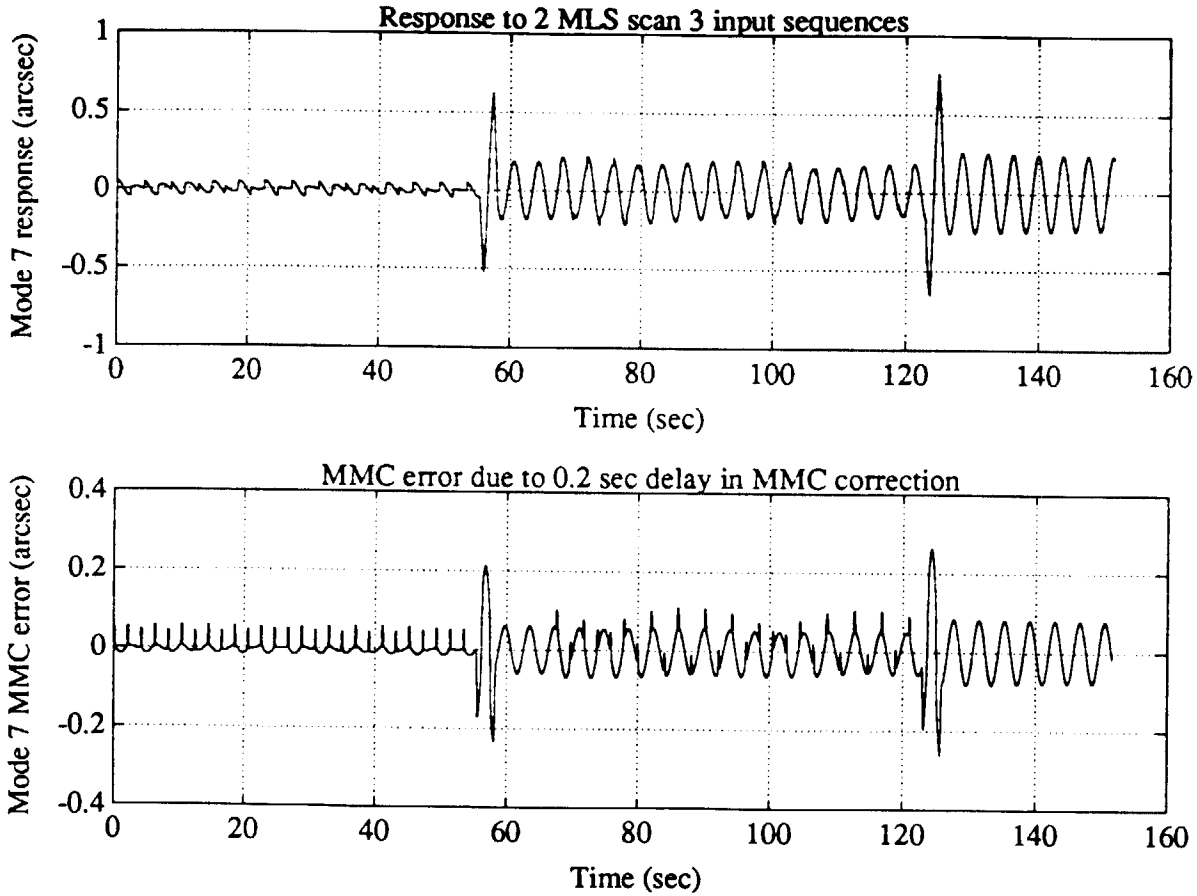

Mode 11 - Effect of MMC Time Delay

This plot shows the response of mode 11of the UARS model at WINDII due to MLS scan 3 pulse sequences, and the residual error due to mode 11 MMC with a 0.2 second time delay.

The MMC approach does not reduce the error magnitude due to this mode where there is a 0.2 second time delay present. This is because the 0.2 second time delay cause almost exactly a 60 degree phase shift in the compensation for this 0.863 Hz mode, so that the subtraction does not reduce the magnitude of the error.

Mode 11 - Effect of MMC Time Delay

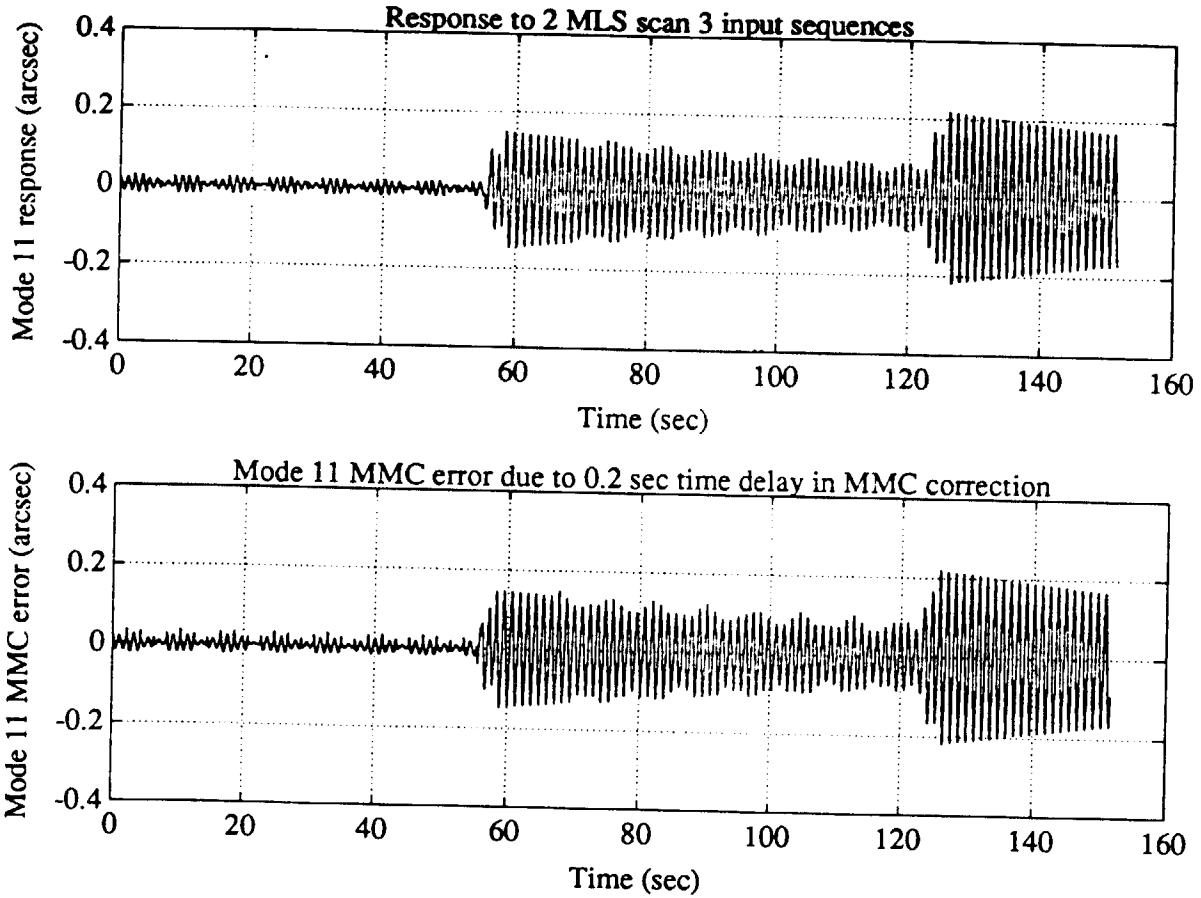

This plot shows the overall pointing error at WINDII due to MLS scan 3 pulse cycles when both the rigid-body response, and the response due to modes 7 and 11, are removed via MMC with a 0.2 second time delay.

Although the MMC performance is degraded over the case when there was no time delay, there is still an advantage to implementing the MMC. Actually, only mode 7 MMC gives the improvement, since the major effect is the reduction of the error spikes at the return pulse times (recall that these spikes are dominated by mode 7 response), whereas the error due to mode 11 MMC is no better than the response of mode 11.

MMC with Time Delay

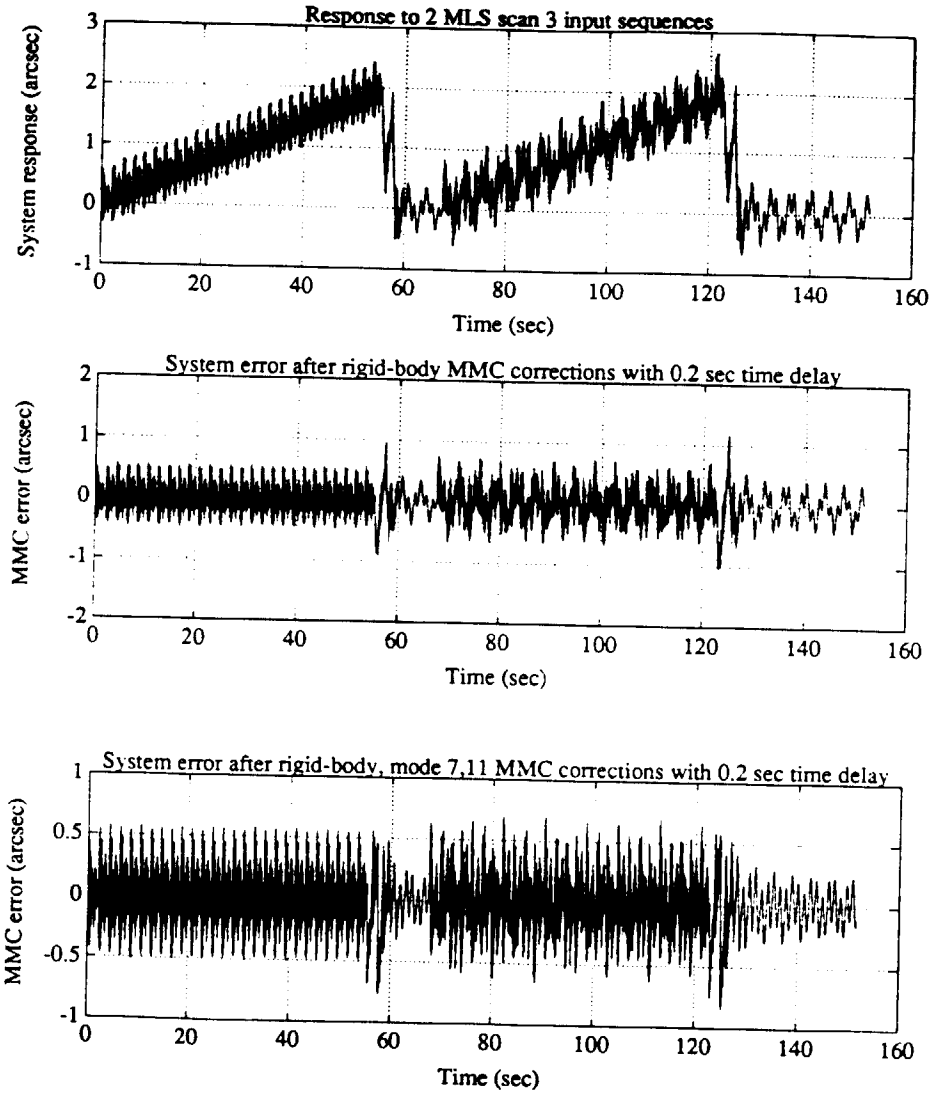

Time Delay Error Magnitude and Phase

Time delay causes a phase shift in the compensation signal. When this time delay phase shift reaches 60 degrees, the relative magnitude of the difference of the signal and its delayed compensation reaches 1.0. This 60 degree phase is obtained when the modal period is six times the time delay. Note that mode 11 has a frequency of 0.843 Hz, which is gives almost exactly a 60 degree phase shift due to a 0.2 second time delay, and explains why there was no error reduction using mode 11 MMC with a 0.2 second time delay (see slide 43).

As the time delay increases past this 60 degree point, the magnitude of the error due to the time delay becomes larger than the signal itself. The error magnitude is only less than the signal magnitude when the time delay is such that the phase difference between the signal and its compensation lies between -60 degrees and 60 degrees.

These plots show the magnitude and phase of the MMC error for a forward pulse with a 0.2 second time delay as a function of the modal frequency, after the compensation has been applied and relative to the original signal.

The upper plot gives $\gamma_{7j}(\omega_j)$ and the lower plot gives $\psi_{7j}(\omega_j)$, both as functions of the modal frequency (see page 49 and the error equations for a forward pulse with flexible-mode MMC with time delay). Note that for a modal frequency of 5 Hz, a 0.2 second time delay corresponds to a 360 degree phase shift. The associated MMC error is not necessarily zero however, since the scan stops and restarts, and the transients are not compensated correctly. This plot indicates the maximum safe frequency for a modal compensation candidate (prior to which the normalized magnitude is less always than one).

Time Delay Error Magnitude and Phase

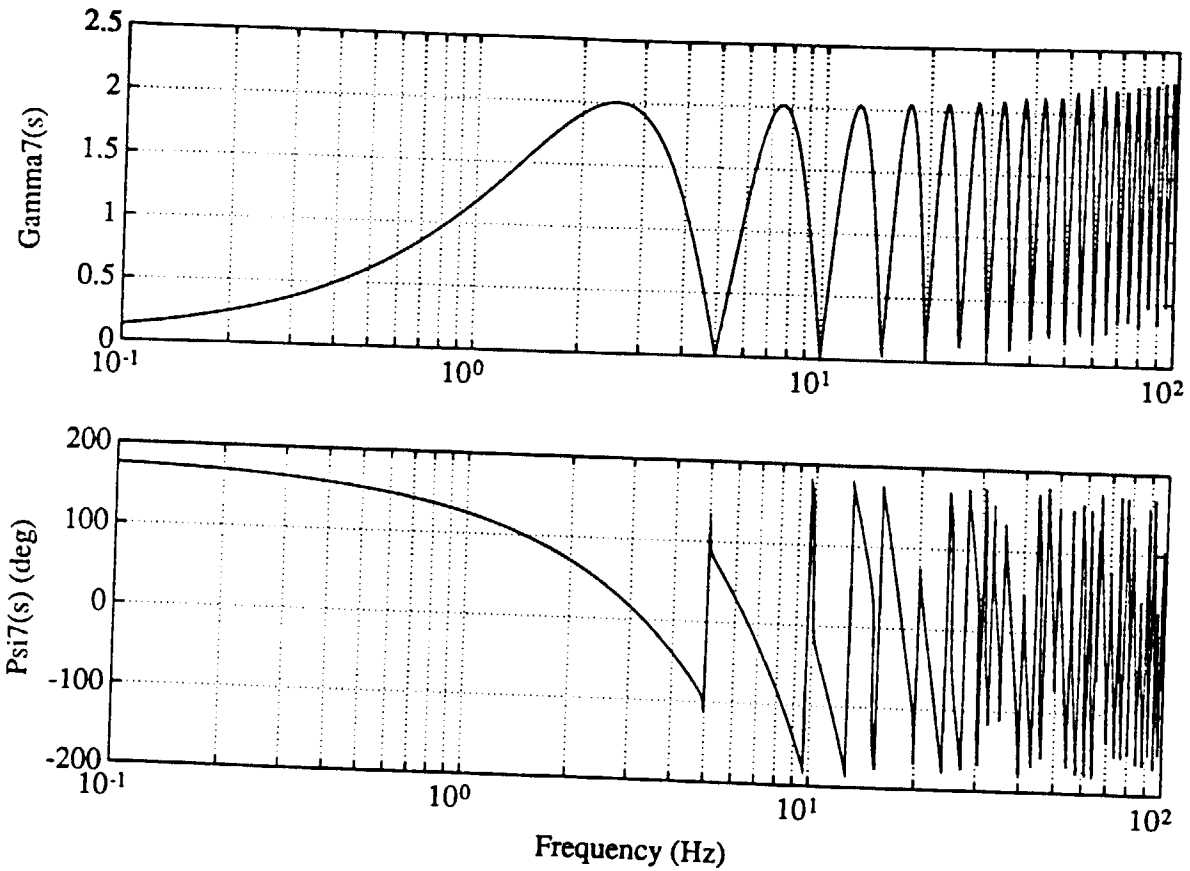

Mode 16 - Effect of MMC Time Delay

This plot shows the response of mode 16 of the UARS model at WINDII due to MLS scan 3 pulse cycles, and the residual error due to mode 16 MMC with a 0.2 second time delay. This plot is included to illustrate the undesirable effect of a time delay on the flex-body MMC performance, even though in this specific example mode 16 was not determined an important mode in the WINDII response to MLS scans.

For this mode, the MMC approach approximately doubles the error magnitude with a 0.2 second time delay. This is because mode 16 has a frequency of 2.113 Hz, which gives about 152 degrees of phase shift due to a 0.2 second time delay. Therefore, the MMC error would be approximately twice the original response.

Mode 16 - Effect of MMC Time Delay

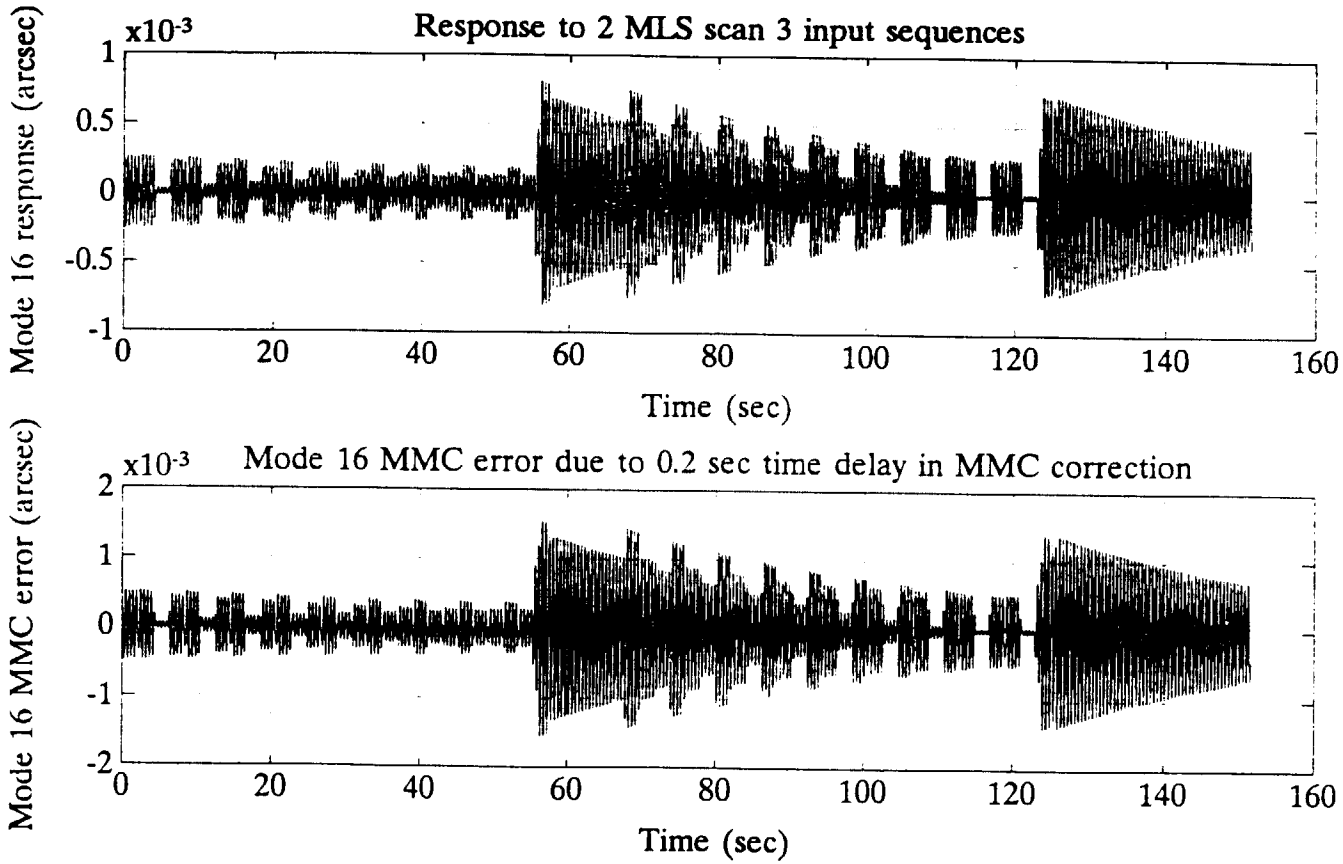

Equations for Rigid-Body MMC with Time Delay

These equations give the residual rigid-body MMC error for a forward pulse sequence due to a time delay of Td seconds in the application of the compensation. As expected, the residual error after the forward pulse duration plus the time delay is zero. The maximum error is independent of the time delay, since the entire pulse ends before the compensation begins.

Equations for Rigid-Body MMC with Time Delay

For a forward pulse: (Td > Tf+T)

$$e_{j_f}(t)=\begin{cases}\frac{1}{2}At^2 & \forall t\varepsilon[0,2T) \\ 2AT(t-T) & \forall t\varepsilon\left[2T,T_f\right) \\ 2AT(t-T)-A\left(t-T_f\right)^2 & \forall t\varepsilon\left[T_f,T_f+T\right) \\ AT\left(2T_f-T\right) & \forall t\varepsilon\left[T_f+T,T_d\right) \\ AT\left(2T_f-T\right)-\frac{1}{2}A\left(t-T_d\right)^2 & \forall t\varepsilon\left[T_d,T_d+2T\right) \\ AT\left[\left(2T_f-T\right)-2\left(t-T_d\right)\right] & \forall t\varepsilon\left[T_d+2T,T_d+T_f\right) \\ AT\left[\left(2T_f-T\right)-2\left(t-T_d\right)\right]+A\left(t-T_f-T_d\right)^2 & \forall t\varepsilon\left[T_d+T_f,T_d+T_f+T\right) \\ 0 & \forall t\geq T_d+T_f+T \end{cases}$$

Equations for Rigid-Body MMC with Time Delay (cont.)

These equations give the residual rigid-body MMC error for a return pulse sequence due to a time delay of Td seconds in the application of the compensation. Again, the residual error after the retrurn pulse duration plus the time delay is zero. The maximum error is now dependent on the time delay, since the compensation begins while the MLS in in the slew part of the return pulse motion.

Equations for Rigid-Body MMC with Time Delay (cont.)

For a return pulse: (2T < Td < Tr)

$$e_{j_r}(t) = \begin{cases} \frac{1}{2}At^2 & \forall t \varepsilon [0, 2T) \\ 2AT(t-T) & \forall t \varepsilon [2T, T_d) \\ 2AT(t-T) - \frac{1}{2}A(t-T_d)^2 & \forall t \varepsilon [T_d, T_d+T) \\ 2AT_dT & \forall t \varepsilon [T_d+T, T_r) \\ 2AT_dT - A(T-T_r)^2 - \frac{1}{2}A(t-T_d)^2 & \forall t \varepsilon [T_r, T_r+T) \\ AT[(2T_r+T) - 2(t-T_d)] & \forall t \varepsilon [T_r+T, T_d+T_r) \\ AT[(2T_r+T) - 2(t-T_d)] + A(t-T_r-T_d)^2 & \forall t \varepsilon [T_d+T_r, T_d+T_r+T) \\ 0 & \forall t \geq T_d+T_r+T \end{cases}$$

Equations for Flexible-Mode MMC with Time Delay

These equations give the residual flexible-mode MMC error for a forward pulse sequence due to a time delay of Td seconds in the application of the compensation. The coefficients used are defined on the next page.

C-2

Equations for Flexible-Mode MMC with Time Delay

For a forward pulse: (Td > Tf+T)

$$e_{j_f}(t) = \frac{A}{\omega_j^2 \sin\phi_j} \begin{cases} \sin\phi_j - e^{-\zeta_j\omega_j t}\sin\left(\omega_{jd}t + \phi_j\right) & \forall t\varepsilon[0,2T) \\ \gamma_{1j}e^{-\zeta_j\omega_j t}\sin\left(\omega_{jd}t + \psi_{1j}\right) & \forall t\varepsilon\left[2T, T_f\right) \\ \gamma_{2j}e^{-\zeta_j\omega_j t}\sin\left(\omega_{jd}t + \psi_{2j}\right) - 2\sin\phi_j & \forall t\varepsilon\left[T_f, T_f + T\right) \\ \gamma_{3j}e^{-\zeta_j\omega_j t}\sin\left(\omega_{jd}t + \psi_{3j}\right) & \forall t\varepsilon\left[T_f + T, T_d\right) \\ \gamma_{4j}e^{-\zeta_j\omega_j t}\sin\left(\omega_{jd}t + \psi_{4j}\right) - \sin\phi_j & \forall t\varepsilon\left[T_d, T_d + 2T\right) \\ \gamma_{5j}e^{-\zeta_j\omega_j t}\sin\left(\omega_{jd}t + \psi_{5j}\right) & \forall t\varepsilon\left[T_d + 2T, T_d + T_f\right) \\ \gamma_{6j}e^{-\zeta_j\omega_j t}\sin\left(\omega_{jd}t + \psi_{6j}\right) + 2\sin\phi_j & \forall t\varepsilon\left[T_d + T_f, T_d + T_f + T\right) \\ \gamma_{3j}\gamma_{7j}e^{-\zeta_j\omega_j t}\sin\left(\omega_{jd}t + \psi_{7j}\right) & \forall t \geq T_d + T_f + T \end{cases}$$

Equations for Flexible-Mode MMC with Time Delay (cont..)

The equations give the coefficients defined in the equations on the pevious page. Note that γ_{1j}, γ_{2j}, γ_{3j}, ψ_{1j}, ψ_{2j}, ψ_{3j} are as defined earlier on slide 23.

Equations for Flexible-Mode MMC with Time Delay (cont.)

$$\gamma_{4j} = \sqrt{\left[\gamma_{3j}\sin\psi_{3j} + e^{\zeta_j\omega_j T_d}\sin\left(\phi_j - \omega_{jd}T_d\right)\right]^2 + \left[\gamma_{3j}\cos\psi_{3j} + e^{\zeta_j\omega_j T_d}\cos\left(\phi_j - \omega_{jd}T_d\right)\right]^2}$$

$$\gamma_{5j} = \sqrt{\left[\gamma_{3j}\sin\psi_{3j} - \gamma_{1j}e^{\zeta_j\omega_j T_d}\sin\left(\psi_{1j} - \omega_{jd}T_d\right)\right]^2 + \left[\gamma_{3j}\cos\psi_{3j} - \gamma_{1j}e^{\zeta_j\omega_j T_d}\cos\left(\psi_{1j} - \omega_{jd}T_d\right)\right]^2}$$

$$\gamma_{6j} = \sqrt{\left[\gamma_{3j}\sin\psi_{3j} - \gamma_{2j}e^{\zeta_j\omega_j T_d}\sin\left(\psi_{2j} - \omega_{jd}T_d\right)\right]^2 + \left[\gamma_{3j}\cos\psi_{3j} - \gamma_{2j}e^{\zeta_j\omega_j T_d}\cos\left(\psi_{2j} - \omega_{jd}T_d\right)\right]^2}$$

$$\gamma_{7j} = \sqrt{\left[\sin\psi_{3j} - e^{\zeta_j\omega_j T_d}\sin\left(\psi_{3j} - \omega_{jd}T_d\right)\right]^2 + \left[\cos\psi_{3j} - e^{\zeta_j\omega_j T_d}\cos\left(\psi_{3j} - \omega_{jd}T_d\right)\right]^2}$$

$$\psi_{4j} = \tan^{-1}\left[\frac{\gamma_{3j}\sin\psi_{3j} + e^{\zeta_j\omega_j T_d}\sin\left(\phi_j - \omega_{jd}T_d\right)}{\gamma_{3j}\cos\psi_{3j} + e^{\zeta_j\omega_j T_d}\cos\left(\phi_j - \omega_{jd}T_d\right)}\right]$$

$$\psi_{5j} = \tan^{-1}\left[\frac{\gamma_{3j}\sin\psi_{3j} - \gamma_{1j}e^{\zeta_j\omega_j T_d}\sin\left(\psi_{1j} - \omega_{jd}T_d\right)}{\gamma_{3j}\cos\psi_{3j} - \gamma_{1j}e^{\zeta_j\omega_j T_d}\cos\left(\psi_{1j} - \omega_{jd}T_d\right)}\right]$$

$$\psi_{6j} = \tan^{-1}\left[\frac{\gamma_{3j}\sin\psi_{3j} - \gamma_{2j}e^{\zeta_j\omega_j T_d}\sin\left(\psi_{2j} - \omega_{jd}T_d\right)}{\gamma_{3j}\cos\psi_{3j} - \gamma_{2j}e^{\zeta_j\omega_j T_d}\cos\left(\psi_{2j} - \omega_{jd}T_d\right)}\right]$$

$$\psi_{7j} = \tan^{-1}\left[\frac{\sin\psi_{3j} - e^{\zeta_j\omega_j T_d}\sin\left(\psi_{3j} - \omega_{jd}T_d\right)}{\cos\psi_{3j} - e^{\zeta_j\omega_j T_d}\cos\left(\psi_{3j} - \omega_{jd}T_d\right)}\right]$$

These equations give the residual flexible-mode MMC error for a return pulse sequence due to a time delay of Td seconds in the application of the compensation. The coefficients used are defined on the next page.

Equations for Flexible-Mode MMC with Time Delay (cont.)

For a return pulse: (2T < Td < Tr)

$$e_{j_r}(t) = \frac{A}{\omega_j^2 \sin\phi_j} \begin{cases} \sin\phi_j - e^{-\zeta_j\omega_j t}\sin\left(\omega_{jd}t + \phi_j\right) & \forall t\varepsilon[0,2T) \\ \gamma_{1j}e^{-\zeta_j\omega_j t}\sin\left(\omega_{jd}t + \psi_{1j}\right) & \forall t\varepsilon[2T,T_d) \\ \gamma_{8j}e^{-\zeta_j\omega_j t}\sin\left(\omega_{jd}t + \psi_{8j}\right) - \sin\phi_j & \forall t\varepsilon[T_d,T_d+T) \\ \gamma_{1j}\gamma_{9j}e^{-\zeta_j\omega_j t}\sin\left(\omega_{jd}t + \psi_{9j}\right) & \forall t\varepsilon[T_d+T,T_r) \\ \gamma_{10j}e^{-\zeta_j\omega_j t}\sin\left(\omega_{jd}t + \psi_{10j}\right) - 2\sin\phi_j & \forall t\varepsilon[T_r,T_r+T) \\ \gamma_{5j}e^{-\zeta_j\omega_j t}\sin\left(\omega_{jd}t + \psi_{5j}\right) & \forall t\varepsilon[T_r+T,T_d+T_r) \\ \gamma_{6j}e^{-\zeta_j\omega_j t}\sin\left(\omega_{jd}t + \psi_{6j}\right) - 2\sin\phi_j & \forall t\varepsilon[T_d+T_r,T_d+T_r+T) \\ \gamma_{3j}\gamma_{7j}e^{-\zeta_j\omega_j t}\sin\left(\omega_{jd}t + \psi_{7j}\right) & \forall t \geq T_d+T_r+T \end{cases}$$

Equations for Flexible Mode MMC with Time Delay (cont.)

The equations give the coefficients defined in the equations on the pevious page. Note that γ_{1j} thru γ_{7j}, and ψ_{1j} thru ψ_{7j} are as defined earlier.

Equations for Flexible-Mode MMC with Time Delay (cont.)

$$\gamma_{8j} = \sqrt{\left[\gamma_{1j}\sin\psi_{1j} + e^{\zeta_j\omega_j T_d}\sin\left(\phi_j - \omega_{jd}T_d\right)\right]^2 + \left[\gamma_{1j}\cos\psi_{1j} + e^{\zeta_j\omega_j T_d}\cos\left(\phi_j - \omega_{jd}T_d\right)\right]^2}$$

$$\gamma_{9j} = \sqrt{\left[\sin\psi_{1j} - e^{\zeta_j\omega_j T_d}\sin\left(\psi_{1j} - \omega_{jd}T_d\right)\right]^2 + \left[\cos\psi_{1j} - e^{\zeta_j\omega_j T_d}\cos\left(\psi_{1j} - \omega_{jd}T_d\right)\right]^2}$$

$$\gamma_{10j} = \sqrt{\left[\gamma_{1j}\gamma_{9j}\sin\psi_{9j} + 2e^{\zeta_j\omega_j T_r}\sin\left(\phi_j - \omega_{jd}T_r\right)\right]^2 + \left[\gamma_{1j}\gamma_{9j}\cos\psi_{9j} + 2e^{\zeta_j\omega_j T_r}\cos\left(\phi_j - \omega_{jd}T_r\right)\right]^2}$$

$$\psi_{8j} = \tan^{-1}\left[\frac{\gamma_{1j}\sin\psi_{1j} + e^{\zeta_j\omega_j T_d}\sin\left(\phi_j - \omega_{jd}T_d\right)}{\gamma_{1j}\cos\psi_{1j} + e^{\zeta_j\omega_j T_d}\cos\left(\phi_j - \omega_{jd}T_d\right)}\right]$$

$$\psi_{9j} = \tan^{-1}\left[\frac{\sin\psi_{1j} - e^{\zeta_j\omega_j T_d}\sin\left(\psi_{1j} - \omega_{jd}T_d\right)}{\cos\psi_{1j} - e^{\zeta_j\omega_j T_d}\cos\left(\psi_{1j} - \omega_{jd}T_d\right)}\right]$$

$$\psi_{10j} = \tan^{-1}\left[\frac{\gamma_{1j}\gamma_{9j}\sin\psi_{9j} + 2e^{\zeta_j\omega_j T_r}\sin\left(\phi_j - \omega_{jd}T_r\right)}{\gamma_{1j}\gamma_{9j}\cos\psi_{9j} + 2e^{\zeta_j\omega_j T_r}\cos\left(\phi_j - \omega_{jd}T_r\right)}\right]$$

If the scanning payload (mirror) becomes larger, there will be a corresponding increase in the payload inertia. The disturbance torques generated from the scanning motion are directly porportional to the inertia of the scanning device. The relationship between the size of the scanning mirror and the generated disturbance is highly nonlinear. The analysis here shows the expected inertia increase is proportional to the fifth power of the size.

However, it should be possible to reduce the mass from that predicted using intelligent design methods. Therefore, assume that the inertia (disturbance) increase is proportional to the size to the power of 4.5. Hence, a scanning mirror three times larger will lead to a disturbance that is approximately 140 times larger, if all other scanning parameters (slew rate, scan angle) are constant.

Effect of Larger Disturbances

Consider the case when the slewing payload (MLS in this case) becomes three times larger, while the spacecraft mass, payload slew rate, and scan angle are constant.

$$\text{Inertia} \sim (\text{mass})(\text{dimension})^2$$

$$(\text{mass}) \sim (\text{density})(\text{dimension})^3$$

$$\Rightarrow \text{Inertia} \sim (\text{density})(\text{dimension})^{4.5}$$

The resultant disturbances will increase by a factor of approximately 140.

MMC Error with Larger Disturbance

These plots show the baseline pointing error (X-axis responses at WINDII to two MLS scan 3 pulse cycles) when the MLS scanning mirror is three times its nominal size. The upper plot shows the rigid-body response and the lower plot shows the total rigid+flex body response.

Compare these to slide 15, which shows the same error plots for the nominal case. Note that now the maximum pointing error is approximately 0.1 deg.

MMC Error with Larger Disturbance

- scanning mirror increased in size by a factor of 3

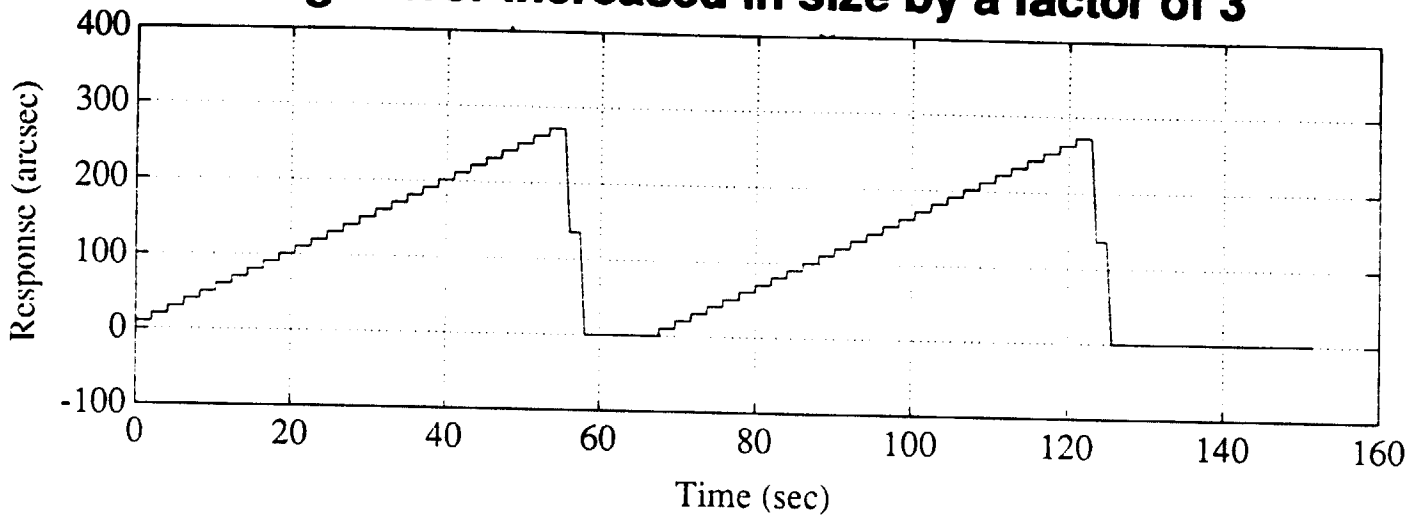

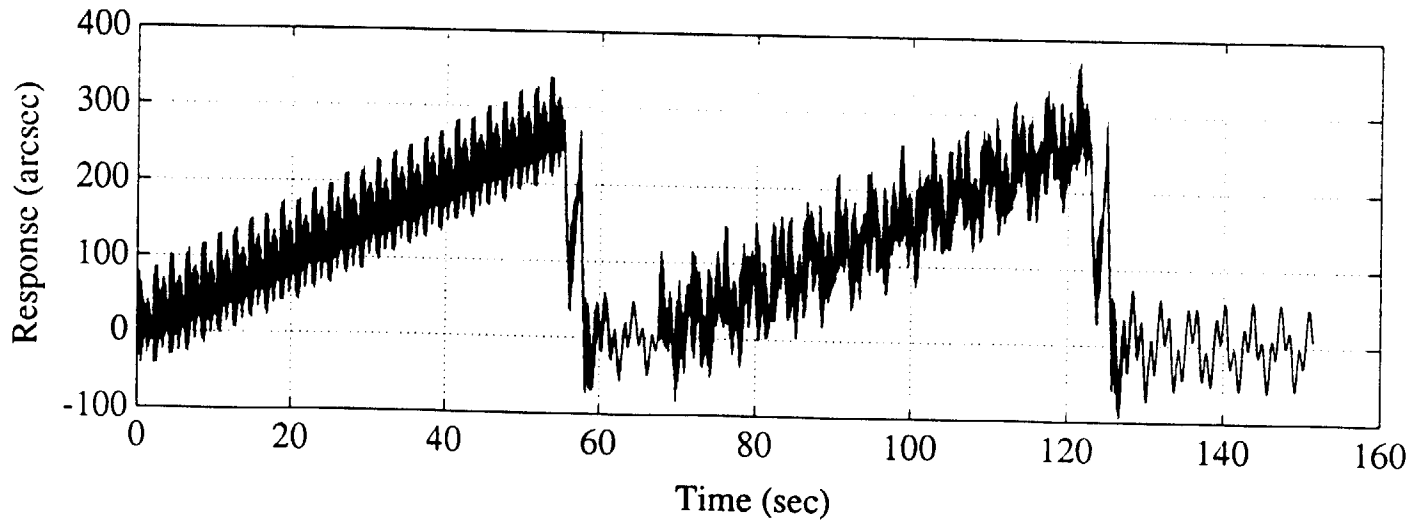

If the scanning mirror is so large as to produce 0.1 degrees of pointing error when the required accuracy is in the low arcsecond range, momentum compensation at the disturbance source is recommended. Momentum compensation would produce (nominally) a balancing torque to the scanning mirror disturbance, at the cost of a possibly large mass penalty (for examples, see JPL work in AIAA 88-4179-CP).

It is unclear how accurate a momentum compensation system would be. It seems unlikely that it would far surpass the currently achievable compensation capabilities of either feedforward or feedback compensation. Feedback can decrease the error by a factor of 10 or more, feedforward has shown a factor of 15 improvement (for GOES I/M), so that an optimistic prediction for momentum compensation would be a factor of 30 improvement in the error (3% momentum compensation "leakage"). For a scanning mirror increased to three times the nominal size, a 3% leakage still results in a factor of 4.2 increase in pointing error.

Another disturbance avoidance technique involves input torque shaping. Torque pulse smoothing reduces the commanded disturbance bandwidth while changing the torque pulse timing can help attenuate disturbance response by appropriate deadbeating of the major modal components. Note that GE has already altered the shape of the return pulse once to reduce the solar array excitations.

Disturbance Avoidance

With a 140-fold increase in disturbance, recommend minimizing the disturbance torques using:

- Momentum compensation at the source.
  - can be costly in mass (additional ~20 kg, see JPL MMII work).
  - achievable accuracy dependent on momemtum exchange leakage (3% leakage still gives 4x increase in disturbance torques).
- Input torque shaping (may get customer reluctance).
  - choose torque pulse shapes to reduce excitation bandwidth (smoothing).
  - choose torque pulse timing to reduce undesirable flex mode excitation (disturbance deadbeat).

Feedforward compensation of flexible modes is sensitive to modelling accuracy (knowledge of flexible mode frequency, mode shapes, and damping), but not to sensor performance (open loop - no sensor).

Feedback compensation is sensitive to sensor performance (bandwidth, noise, sampling rate) but not to modelling accuracy (since no system modelling is used in direct feedback of sensor measurements).

Feedback compensation can be used alone or with feedforward compensation. The current task is to determine the limitations of both approaches, and how they compare to the use of MMC type feedforward compensation alone.

Use of Feedback Compensation

- Feedforward compensation of flexible modes sensitive to modelling accuracy: no sensor involved.
- Feedback compensation is sensitive to sensor performance: no model involved.
- Feedback compensation can be used alone, e.g. Image Motion Compensation (for UIT)
- Feedback can be used together with MMC feedforward compensation.

UARS Roll Axis Normal Mode Controller

This slide shows the UARS roll axis normal mode control system, as designed by GE, and drawn here for an MLS disturbance input and WINDII output. This loop is intended to provide rigid-body control only, and is decoupled from the pitch and yaw axis controllers. The controller has the following properties:

- Modified PID control law with zero steady-state error to disturbance torque inputs.
- Control law executed and wheel commands sent every 0.512 sec.
- Consider worst case 0.512 sec. delay for both gyro data input to control law and commanded wheel output.
- Gyro data sampled every 0.128 sec to reduce aliasing of structural resonant frequencies.
- Digital prefilter is two simple lags at 0.5 Hz.
- Controller block equivalent to 3 simple lags at 0.007 rad/s and 2 simple lags at 0.3 rad/s.
- Wheel loop bandwidth is 0.02 rad/s.
- Structural mode damping assumed at 0.002.
- Gyro parameters assumed: 2 Hz. bandwidth, damping 0.5.

UARS Roll Axis Normal Mode Controller

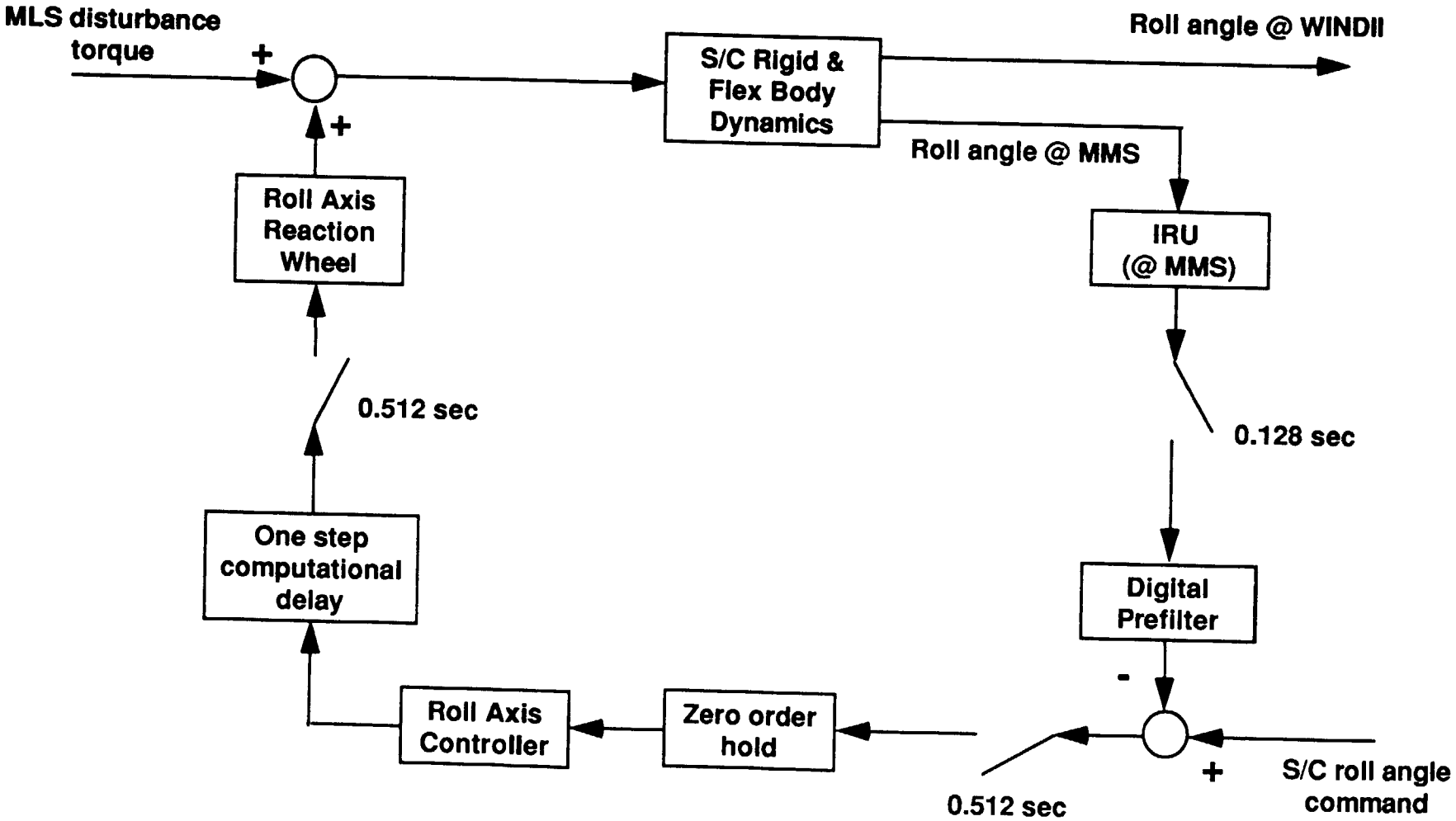

Baseline Pointing Error with Normal Mode Control

This plot shows the effect of the UARS normal mode control law on the baseline pointing error at WINDII due to MLS disturbances. Compared to slide 15, which shows the same error without the normal mode control, note the following points:

- The rigid-body contribution to the pointing error averaged to zero by the rigid-body control.
- Baseline pointing error due to large disturbance effects of the 2 MLS return pulses at the end of each cycle is not improved significantly because the disturbance is impulsive.
- The normal mode control law bandwidth of 0.007 rad/s is too low to actively control any flexible mode (where the first flexible mode has a frequency of approximately 1.2 rad/s).

Baseline Pointing Error with Normal Mode Control

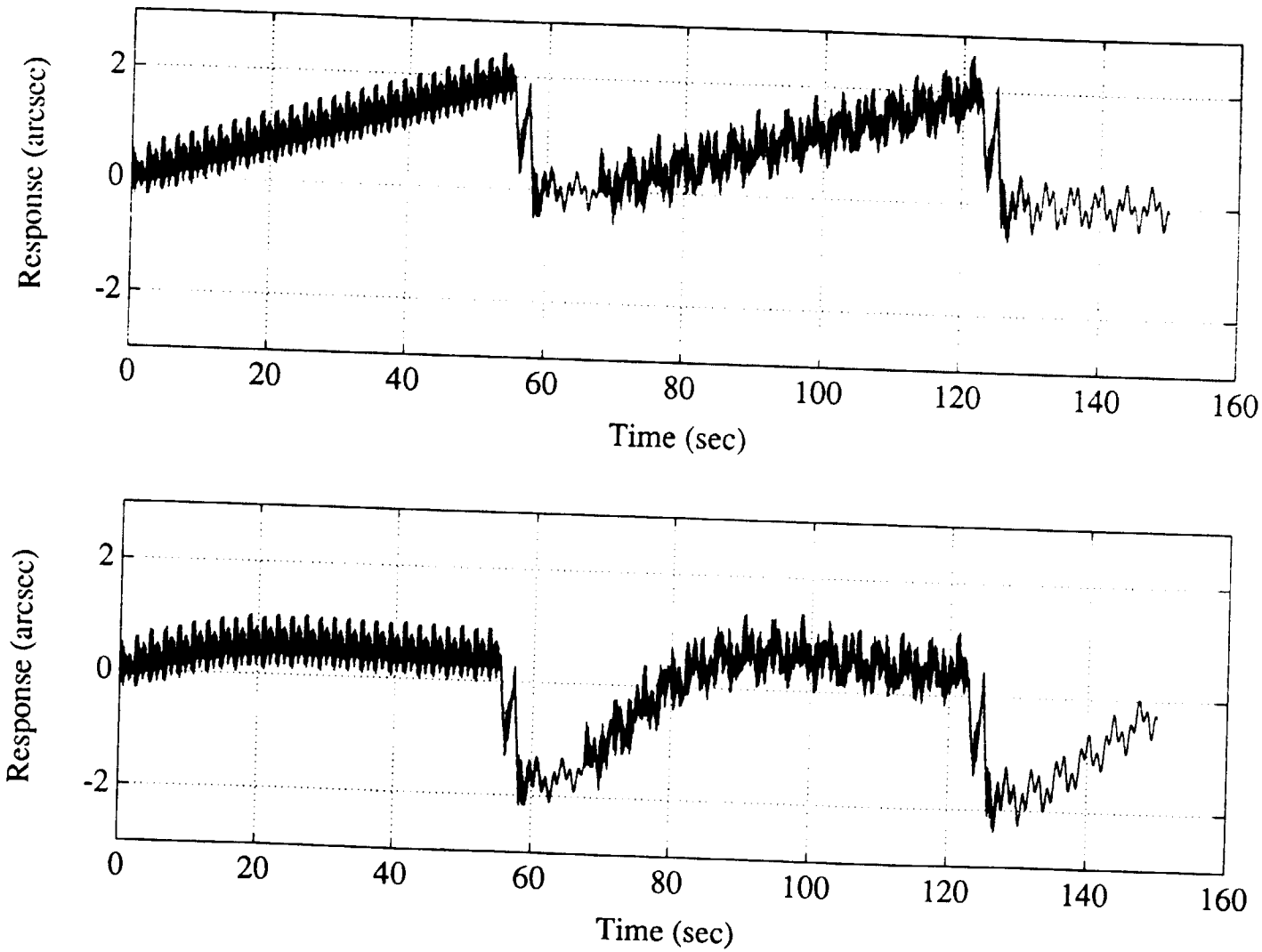

This slide gives a block diagram representation of a direct feedback compensation scheme at WINDII for disturbances due to the MLS scans. On UARS, the gyros (IRU) are located on the MMS. Therefore, WINDII feedback is using measurements from a separate location. This presents no problems for low order modes (which are the most dominant in our particular case), but high order modes (non-appendage modes) may produce different components at MMS than at WINDII, rendering their feedback compensation inappropriate.

The gyros are sampled once every T seconds. This sample rate must be determined based on the capability of the on-board electronics and with a mind to the sensor characteristics. For example, current UARS gyros have a bandwidth of 2 Hz, so that it would make no sense to sample them faster than the corresponding Nyquist frequency of 1 Hz. The gyro is modelled as a second order system with cutoff frequency of the 2 Hz and damping ratio 0.5.

Direct Feedback Compensation at WINDII

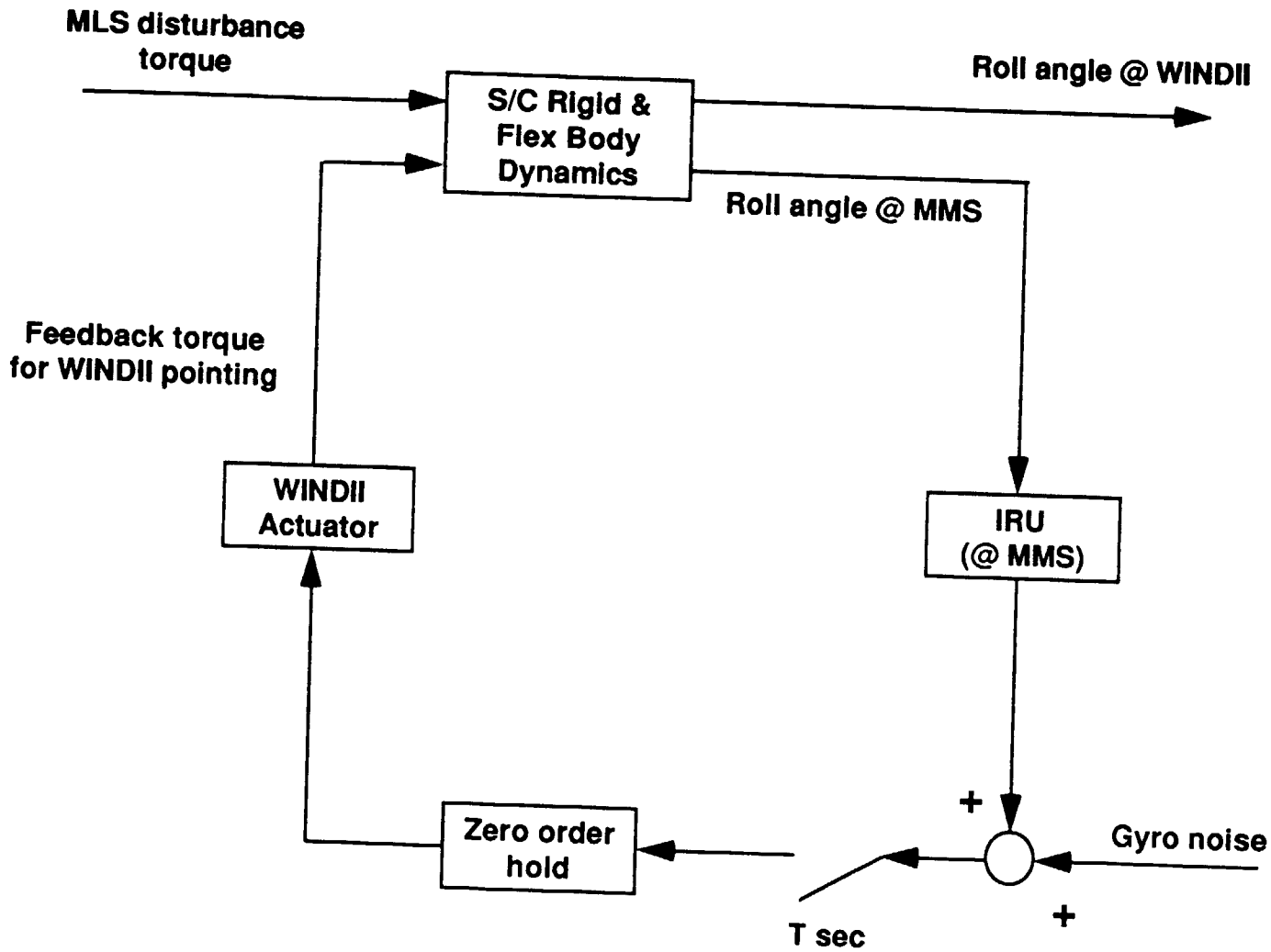

Pointing Error with Direct Feedback Compensation

The upper plot shows the baseline pointing error while the lower plot shows the pointing error when WINDII is controlled via direct feedback of the attitude from the MMS gyros with noise added. The gyro noise was obtained from actual gyro test data for gyros whose specification was 0.03 deg/h in 6 hours (3 sigma). The gyro sample time T is assumed to be 0.2 seconds. Note that the current UARS roll-axis control loop is sampled every 0.512 seconds, and this lower time delay was used for comparison with the 0.2 second time delay simulated using feedforward MMC in slide 44.

The maximum pointing error has been reduced by more than a factor of 2, from 2.7 arcsec to approximately 1.1 arcsec. This error is due to the time delay in applying the control through the sample and hold gyro measurement circuit. In this respect, both feedback and feedforward compensation are affected in a similar fashion by any time delays in the system (compare with slide 44). For a digital control system, time delays are inevitable.

Usually time delays can lead to instability in a feedback system. Here the controlled part (payload mirror or antenna) is a very small portion of the S/C so that we do not need to worry about any instability in this case.

Pointing Error with Direct Feedback Compensation

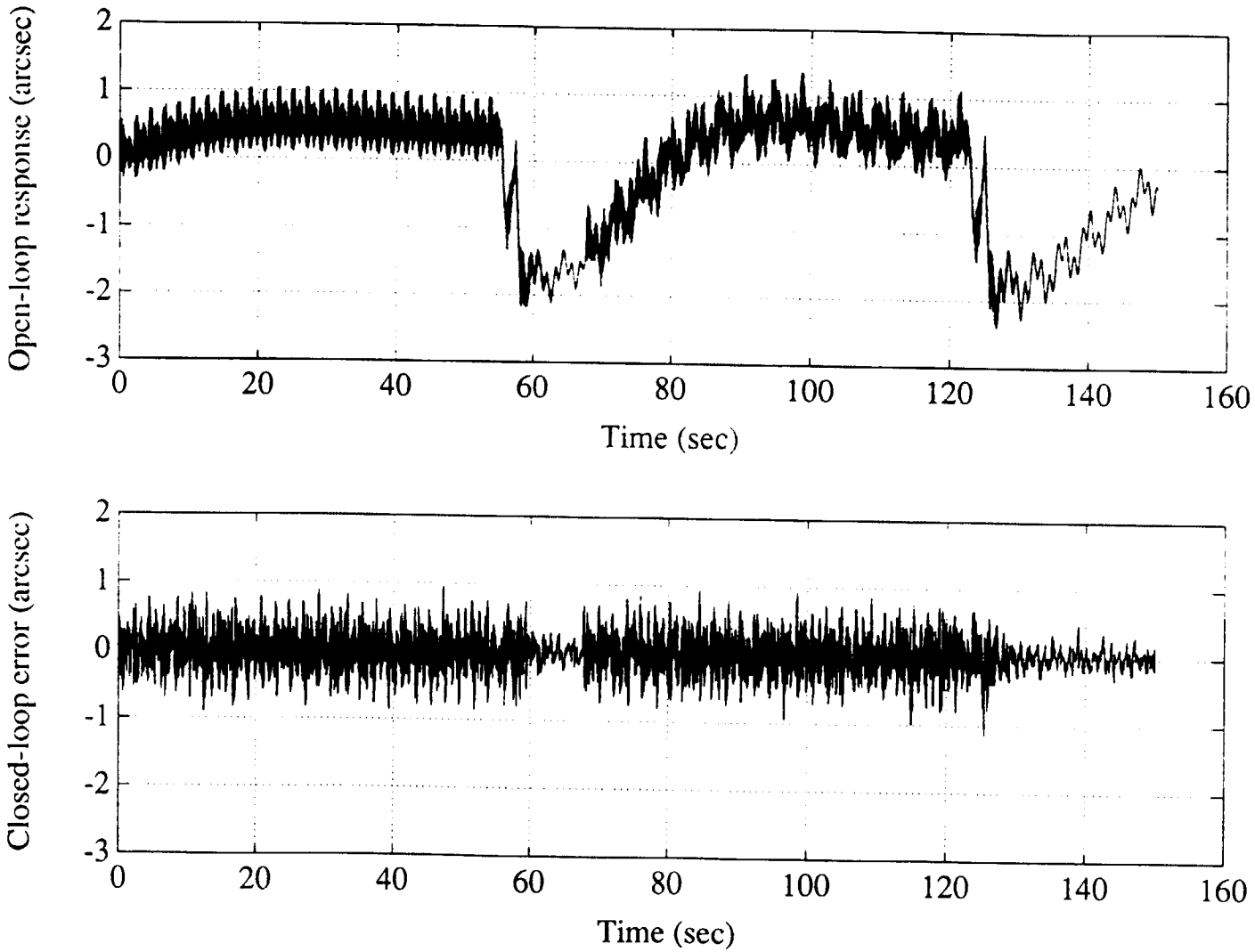

Effect of Sensor Performance

Deficiencies in the performance of the sensor will degrade the feedback compensation of the payload motion.

- The sensor bandwidth effectively reduces the high frequency content of the information in the measurement. Feedback compensation will therefore not compensate for those modes that lie outside the sensor bandwidth and significantly contribute to the motion at any particular payload.
- Any noise generated in the sensor measurement (such as gyro random drift components) will be fed directly into the compensation of payload motion, and will directly affect the residual error.
- Any sensor bias will be fed directly through into the compensation, with a resulting bias on the compensated payload LOS.
- Time delays in the measurement degrade the feedback compensation performance for the same reasons as for MMC. For feedback compensation, high frequency components in the measurement signal will be amplified by a large enough time delay, regardless of relative significance to payload.

Effect of Sensor Performance

- Measurement and compensation of flexible modes not possible outside sensor bandwidth.
- Sensor noise will degrade feedback compensation performance.
- Sensor measurement bias will appear in the residual payload pointing error.
- Time delay degrades feedback compensation performance. Maximum time delay inversely proportional to largest frequency component in measurement.

The feedforward MMC scheme is sensitive to the model used to predict the payload motion. No sensor is used however, so that MMC is not sensitive to any sensor performance deficiencies. Feedback compensation, on the other hand, is insensitive to any system dynamic modelling errors since no system model is used, but is sensitive to the characteristics of the particular sensor used. Feedback compensation can fully replace the function of the MMC, at the cost of the necessary high quality sensors at the appropriate locations.

The MMC scheme is not necessarily redundant if feedback compensation is possible. There remains a subset of problems for which feedback and MMC are both useful and can complement each other.

- If the sensor is unavailable for measurement on a continuous basis (due to power, thermal, life or FOV constraints for example), MMC can be used to provide motion compensation during these periods.
- If the sensor characteristics provide only poor quality measurements (high signal-to-noise ratio for example), the repeatability of the disturbance can be used to filter the sensor measurements to identify system modelling parameters of interest.
- If the sensor placement on the structure precludes the appropriate measurement of any flexible mode of significance to a particular payload disturbance response, MMC can be used to provide compensation of the modal motion for this particular payload. An example would be for a boom (non-appendage) mode of the Space Station when there is no payload dedicated sensor, but only one separated from the payload by a flexible path.
- An MMC scheme can be used as a backup mode for the sensor feedback if redundant sensors are too expensive.

Sensors and Feedback with MMC

- **Feedback compensation can replace MMC if the proper sensor is available/affordable.**

- **MMC can complement direct sensor feedback compensation when:**
  - sensor measurement is not continuously available - part-time sensor can be used to identify modal parameters of interest.
  - sensor noise is large - can use repeatability of disturbances to extract information over time (system identification).
  - sensor placement inappropriate to capture all modes of importance.
  - can be used as backup mode to sensor feedback - degraded science better than no science.

Sensors and Feedback with MMC (cont).

This block diagram gives a schematic for how feedback and MMC would work together in one system. The "Complementary Filter" is so named because it takes signals (from the sensor and from the MMC model) which have strengths and weaknesses that complement each other. The logic contained in the complementary filter would depend on the specific application in hand. For example, if sensor feedback is to be used for system identification, the complementary filter would contain the necessary data reduction and identification algorithms, and may be on the ground or on-board.

Two functions, such as system identification work to improve MMC, and direct feedback compensation, might be included in one complementary filter.

Sensors and Feedback with MMC (cont).

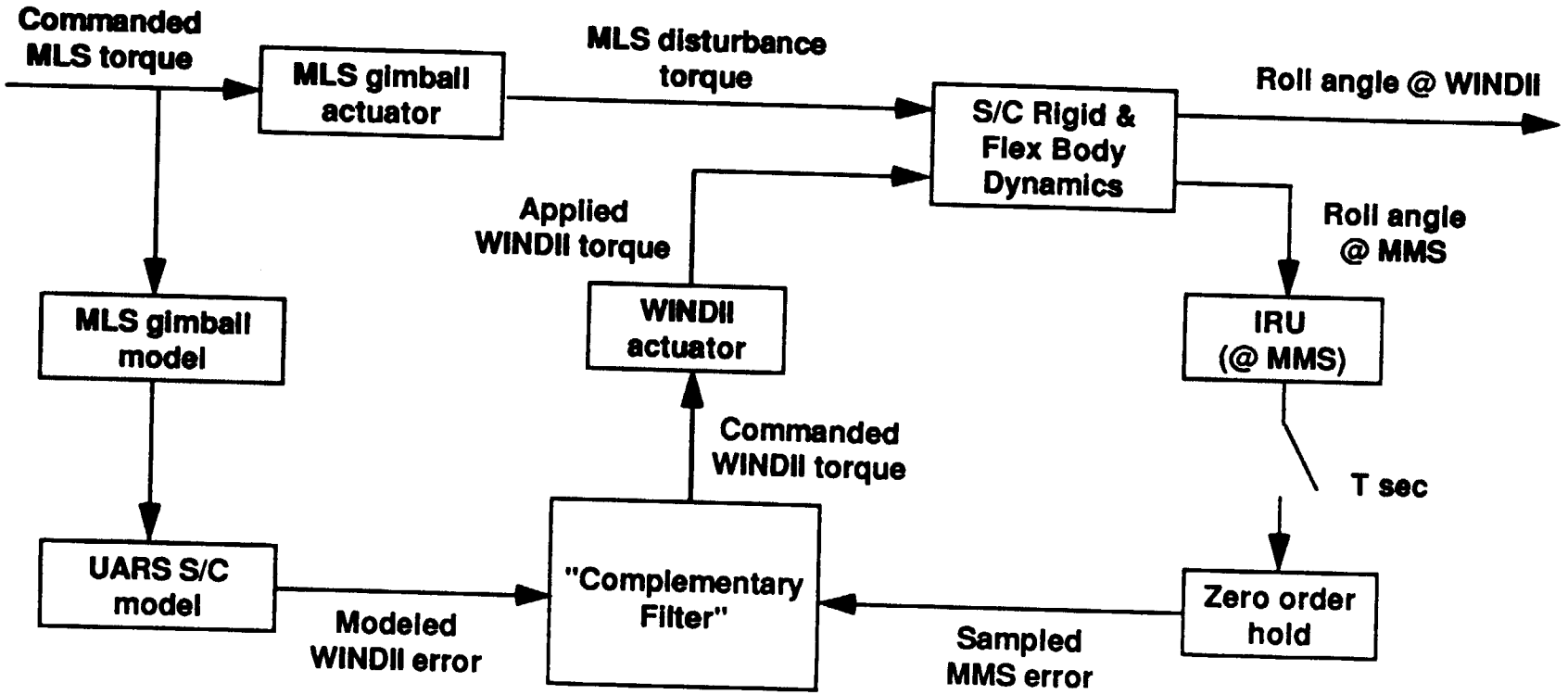

Summary

- Rigid-body response to disturbance eliminated.
- Modal importance to specific input profile helps determine the required complexity of flex mode logic.
- MMC sensitive to system dynamic model fidelity.
- To significantly reduce pointing errors by applying flexible-body MMC, system ID is required to accurately obtain the modal parameters of interest in the following priority:
  - modal frequency
  - modal residue (including system inertia)
  - damping
- Modal damping least important to MMC (contrast to feedback).

Summary (cont).

- Disturbance torque (hence payload pointing error) increases nonlinearly with the scanning mirror size (~size$^{4.5}$).
- Feedback compensation of payload disturbance sensitive to sensor performance limitations.
- If sufficiently rich sensor measurements available, feedback compensation is preferrable to MMC.
- If sufficiently rich sensor measurements are not available, MMC and feedback compensation can work together to provide overall compensation requirements.
- Time delay affects MMC and feedback compensation equally.

Recommendations

- Improve on-orbit ID capability using on-board measurements
  - required for future missions, using either MMC or feedback, due to inadequate modelling tools and ground test errors.
  - modal frequencies, system inertia, most important. Only few modes of interest.
  - Reconcile real on-orbit data with system model parameters(UARS)
- Verify MMC experimentally on realistic flexible test article with realistic controller hardware.
- Investigate methods to minimize the flexible-body interactions at the source:
  - momentum compensation
  - input torque shaping

REPORT DOCUMENTATION PAGE

Form Approved
OMB No. 0704-0188

1. AGENCY USE ONLY *(Leave blank)*	2. REPORT DATE	3. REPORT TYPE AND DATES COVERED
	September 1992	Contractor Report

4. TITLE AND SUBTITLE
Control-Structure Interaction/Mirror Motion Compensation

5. FUNDING NUMBERS
C NAS1-19242
WU 590-14-41-01

6. AUTHOR(S)
Mark McLaren, Peter Chu, Xen Price

7. PERFORMING ORGANIZATION NAME(S) AND ADDRESS(ES)
Space Systems/Loral
3825 Fabian Way
Palo Alto, CA 94303

8. PERFORMING ORGANIZATION REPORT NUMBER

9. SPONSORING / MONITORING AGENCY NAME(S) AND ADDRESS(ES)
National Aeronautics and Space Administration
Langley Research Center
Hampton, VA 23665-5225

10. SPONSORING / MONITORING AGENCY REPORT NUMBER
NASA CR-189672

11. SUPPLEMENTARY NOTES
Langley Technical Monitor - William L. Grantham
Final Report - Task 1

12a. DISTRIBUTION / AVAILABILITY STATEMENT
Unclassified - Unlimited
Subject Category 18

12b. DISTRIBUTION CODE

13. ABSTRACT ***(Maximum 200 words)***

Space Systems/Loral (formerly Ford Aerospace, Space Systems Division) has implemented a rigid-body Mirror Motion Compensation (MMC) scheme for the GOES-I/M spacecraft currently being built for NASA and NOAA. This has resulted in a factor of 15 reduction in pointing error due to rigid-body spacecraft motion induced by the periodic black-body calibration maneuvers required for the instruments. For GOES the spacecraft and the payload mirrors are considered as rigid bodies. The structural flexibility effects are small and are included in the total pointing budget as a separate item.

This paper extends the MMC technique to include structural flexibility. For large multi-payload platforms, the structural flexibility effects can be more important in sensor pointing jitter as the result of payload motion. Sensitivity results are included to show the importance of the dynamic model fidelity.

14. SUBJECT TERMS
Spacecraft pointing jitter, Feed Forward Compensation, Precision Pointing

15. NUMBER OF PAGES
129

16. PRICE CODE
A07

17. SECURITY CLASSIFICATION OF REPORT	18. SECURITY CLASSIFICATION OF THIS PAGE	19. SECURITY CLASSIFICATION OF ABSTRACT	20. LIMITATION OF ABSTRACT
Unclassified	Unclassified		